

H
/

H
/

H
R

O

O

O

-
/

-
/

S
-
/

Q-SORT International Conference

Science and Applications of Coherent Electron Beam Manipulation

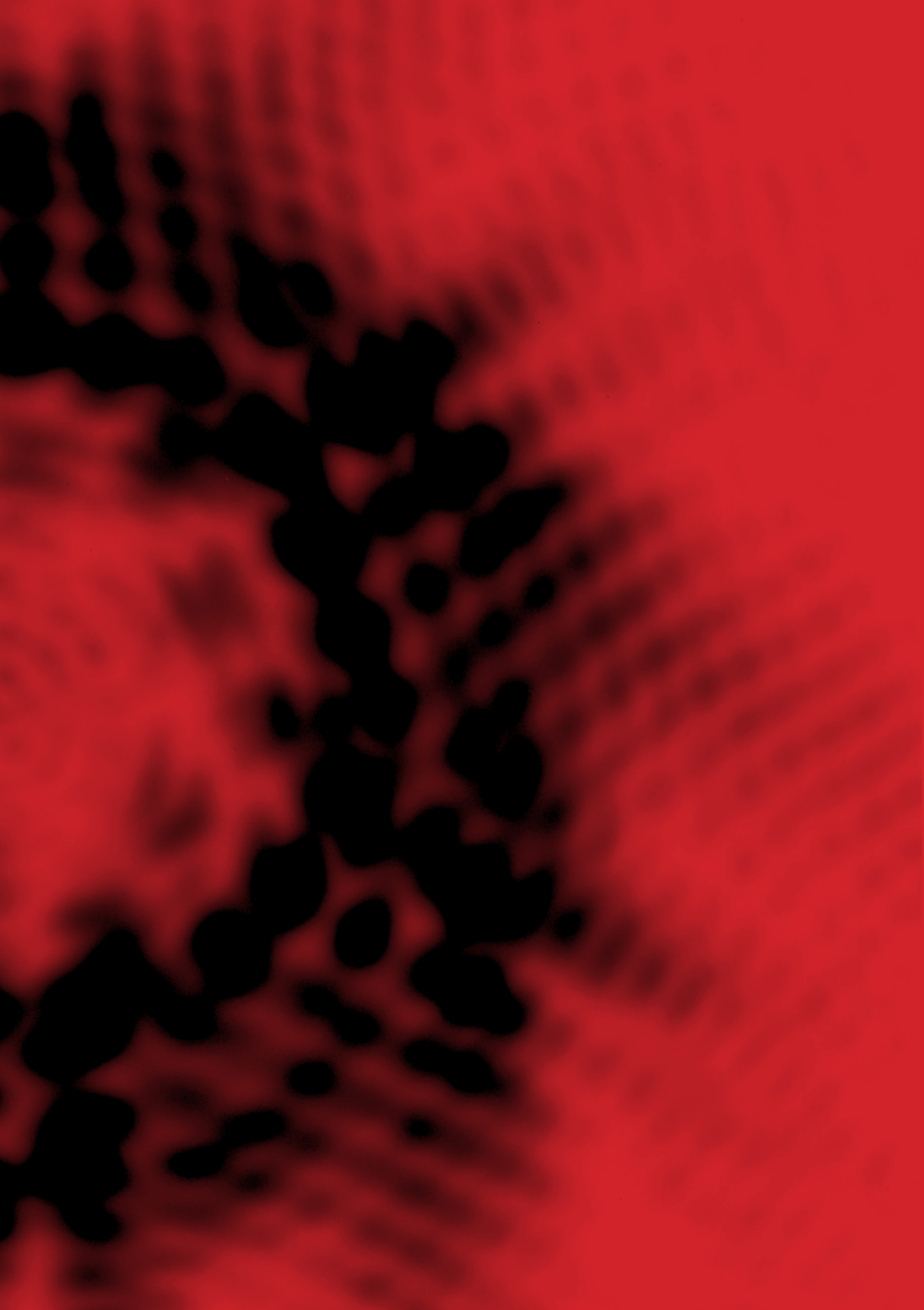
Tuesday 1 — Friday 3
September 2021

Horizon 2020
Framework Programme

Projects:
766970 - Q-SORT
101035013 - MINEON
964591- SMART ELECTRON



This project has received funding from the European Union's Horizon 2020 research and innovation programme under Grant Agreement No. 766970



Programme

- p. 10 Wednesday 1 September
- p. 11 Thursday 2 September
- p. 12 Friday 3 September

Abstracts

- p. 18 Novel developments in 2D and 3D Electron Off-axis Electron Holography
*D. Wolf, A. Lubk
(IFW Dresden, Germany)*
- p. 21 Developments for operando electrical measurements in off-axis electron holography
*J. Dupuy, M.J. Hÿtch, C. Gatel
(CEMES-CNRS, France)*
- p. 22 Phase anti-matching and other semi-crazy ideas
*M. Beleggia
(Technical University of Denmark, Denmark)*
- p. 26 Ptychography & 4D-STEM: Solutions to a big-data problem
*C.T. Koch, M. Schloz, B. Haas, T. Pekin1, J. Müller, G. He, S. Shabih, and W. Van den Broek
(Humboldt-Universität, Germany)*
- p. 28 Field mapping by off-axis electron holography and pixelated STEM
*V. Boureau, M. Staño, D. Cooper
(EPFL, Switzerland)*
- p. 34 Advances in the generation and measurement of structured electromagnetic fields in the transmission electron microscope
A.H. Tavabi, M. Schaaf, M. Kruth, H. Soltner, U. Poppe, P. Rosi, E. Rotunno, A. Roncaglia, L. Belsito, S. Frabboni, G. Pozzi, G.C. Gazzadi, P. Lu, R. Nijland, M. Ghosh, P. Tiemeijer, E. Karimi, V. Grillo, R. E. Dunin-Borkowski
- p. 37 Imaging of complex magnetic textures with particle-like properties
N.S. Kiselev
- p. 38 Ultrafast Spectroscopy from fundamental concepts to applications in magnetism
T. Rasing
- p. 42 Off-axis electron holography and Lorentz microscopy of magnetic skyrmion bubbles in multilayers and van der Waals materials
T. Denneulin, J. Caron, A.H. Tavabi, A. Kovács, R.E. Dunin-Borkowski

p. 48	Segmented- and pixelated-detector differential phase contrast imaging of the iron-rhodium magnetostructural transition	<i>T. Almeida, R. Temple, J. Massey, D. McGrouther, L. Molina, A. Chirkova, K. Skokov, C. H. Marrows, S. McVitie</i>
p. 51	Phase Retrieval by Electron Ptychography	<i>D.A. Muller</i>
p. 56	Electron Energy Loss Spectroscopy with an Orbital Angular Momentum sorter: results and challenges	<i>E. Rotunno</i>
p. 59	Optical polarization analogue in free electrons beams	<i>H. Lourenço-Martins, D. Gérard, M. Kociak</i>
p. 63	Electron beam aberration correction and shaping using optical fields	<i>A. Konečná, F. J. García de Abajo</i>
p. 65	Recent results in 3D wavefront modulation and quantum mechanical detection	<i>T. Latychevskaia, A. Kohli</i>
p. 68	Structured Electron Beams for Interaction-free Measurements and Inelastic Interferometry	<i>B. McMorran, C. Johnson, A. Turner</i>
p. 74	Engineering the wavefunction of electrons for new microscopy methods	<i>F. Carbone</i>
p. 75	Homodyne detection of cathodoluminescence	<i>O. Kfir</i>
p. 77	Complex phase space manipulation of pulsed electron beams in a nanophotonic structure	<i>R. Shiloh, T. Chlouba, J. Illmer, N. Schönenberger, P. Yousefi, A. Tafel, J. Litzel, S. Kraus, L. Brückner, B. Löhr, P. Hommelhoff</i>
p. 78	Tunable Photo-Induced Free-Electron Spatial Modulation	<i>S. Tsesses, R. Dahan, K. Wang, O. Reinhardt, G. Bartal, I. Kaminer</i>
p. 81	Smart Ghost Imaging	<i>F. Grenapin, D. Paneru, T. Guner, A. D'Errico, E. Karimi</i>
p. 86	Towards quantum electron wavepacket spectroscopy in the SEM	<i>A. Polman</i>
p. 89	SMART-electron: Dynamically modulating electrons' wave properties opening new frontiers in electron microscopy	<i>G.M. Vanacore</i>
p. 90	A few new ideas for future directions of microscopy	<i>V. Grillo</i>

Programme

Wednesday 1 September

Zoom

13:40 – 18:30

13:40 – 14:00 • Welcome addresses

Vincenzo Grillo
(National Research Council, Italy)

Session A: Phase and field holography

Chair: David Cooper
(Université Grenoble Alpes, CEA, France)

14:00 – 14:30 A1 – Novel developments in 2D and 3D Electron
Off-axis Electron Holography

Alex Lubk
(IFW Dresden, Germany)

14:30 – 15:00 A2 – Developments for operando electrical
measurements in off-axis electron holography

Christoph Gatel
(CEMES-CNRS, France)

15:00 – 15:30 A3 – Phase anti-matching
and other semi-crazy ideas

Marco Beleggia
(Technical University of Denmark, Denmark)

Session B: Ptychography & 4DSTEM

Chair: David Cooper
(Université Grenoble Alpes, CEA, France)

15:30 – 16:00 B1 – Ptychography & 4D-STEM:
Solutions to a big-data problem

Christoph Koch
(Humboldt-Universität, Germany)

16:00 – 16:30 B2 – Field mapping by off-axis electron holography
and pixelated STEM

Victor Boureau
(EPFL, Switzerland)

16:30 – 17:00 ● Coffee break

Session C: New Magnetic Measurement Ideas

Chair: Rafal Dunin-Borkowski
(Forschungszentrum Jülich, Germany)

17:00 – 17:30 C1 – Advances in the generation and measurement
of structured electromagnetic fields
in the transmission electron microscope

Amir Tavabi
(Forschungszentrum Jülich, Germany)

17:30 – 18:00 C2 – Imaging of complex magnetic textures
with particle-like properties

Nikolai Kiselev
(Forschungszentrum Jülich, Germany)

18:00 – 18:30 C2 – Ultrafast spectroscopy from fundamental
concepts to applications in magnetism

Theo Rasing
(Radboud University, Netherlands)

Thursday 2 September

Zoom

11:00 – 18:30

11:00 – 12:05 • Free discussion-chat

12:15 – 14:00 ● Lunch break

Session D: Phase and field holography

Chair: Rafal Dunin-Borkowski
(Forschungszentrum Jülich, Germany)

14:00 – 14:30 D1 – Off-axis electron holography and Lorentz microscopy of magnetic skyrmion bubbles in multilayers and van der Waals materials

Thibaud Denneulin
(Forschungszentrum Jülich, Germany)

Session E: Ptychography & 4D-STEM

Chair: Rafal Dunin-Borkowski
(Forschungszentrum Jülich, Germany)

14:30 – 15:00 E1 – Segmented- and pixelated-detector differential phase contrast imaging of the iron-rhodium magnetostructural transition

Trevor Almeida
(Université Grenoble Alpes, CEA, France)

15:00 – 15:30 E2 – Phase Retrieval by Electron Ptychography

David Muller
(Cornell University, USA)

15:30 – 16:00 ● Coffee break

Session F: Electron Beam Shaping

Chair: Stefano Frabboni
(Università di Modena e Reggio Emilia, Italy)

16:00 – 16:30 F1 – Electron Energy Loss Spectroscopy with an Orbital Angular Momentum sorter: results and challenges

Enzo Rotunno
(National Research Council, Italy)

16:30 – 17:00 F2 – Optical polarization analogue in free electrons beam

M. Kociak
(Paris Sud, France)

17:00 – 17:30 F3 – Electron beam aberration correction and shaping using optical fields

Andrea Konecna
(ICFO-ICFO-Institut de Ciències Fotoniques, Spain)

17:30 – 18:00 F4 – Recent results in 3D wavefront modulation and quantum mechanical detection

Tatiana Latychevskaia
(Paul Scherrer Institute, Switzerland)

18:00 – 18:30 F5 – Structured Electron Beams for Interaction-free Measurements and Inelastic Interferometry

Benjamin Mc Morran
(University of Oregon, USA)

Friday 1 September

Zoom

11:00 – 19:00

11:00 – 12:05 • Free discussion-chat

Vincenzo Grillo
(National Research Council, Italy)

12:15 – 14:00 ● Lunch break

Session G: Electron-radiation interaction

Chair: Vincenzo Grillo
(National Research Council, Italy)

14:00 – 14:30 G1 – Engineering the wavefunction of electrons
for new microscopy methods

Fabrizio Carbone
(EPFL, Switzerland)

14:30 – 15:00 G2 – Homodyne detection of cathodoluminescence

Ofer Kfir
(University of Tel Aviv, Israel)

15:00 – 15:30 G3 – Complex phase space manipulation of pulsed
electron beams in a nanophotonic structure

Peter Hommelhoff
(Friedrich-Alexander-Universität Erlangen-Nürnberg,
Erlangen, Germany)

15:30 – 16:00 G4 – Tunable Photo-Induced
Free-Electron Spatial Modulation

Shai Tseses
(Technion, Israel)

16:00 – 17:00 G5 – Smart Ghost Imaging

Ebrahim Karimi
(University of Ottawa, Canada)

17:00 – 17:30 ● Coffee break

Session H: Electron-radiation interaction

Chair: Ido Kaminer
(Technion, Israel)

17:30 – 18:00 H1 – Towards quantum electron wavepacket
spectroscopy in the SEM

Albert Polman
(NWO-Institute AMOLF)

18:00 – 18:30 H2 – SMART-electron: Dynamically modulating
electrons' wave properties opening
new frontiers in electron microscopy

Gianmaria Vanacore
(University of Milano-Bicocca, Italy)

18:30 – 19:00 H3 – A Few New Ideas for Future Directions
in Microscopy

Vincenzo Grillo
(National Research Council, Italy)

19:00 • Wrap-up



Abstracts

by first author

Session A:

Phase and field
holography

Novel developments in 2D and 3D Electron Off-axis Electron Holography

D. Wolf¹ and A. Lubk¹

¹*Institute for Solid State and Materials Research (IFW) Dresden, Germany*

Introduction

Off-axis electron holography retrieves the electrostatic and magnetic Aharonov-Bohm phase shift that an electron wave experiences upon passing a sample, which may be related to the projected electric field \mathbf{E} and magnetic flux density \mathbf{B} in the sample under so-called kinematic imaging or scattering conditions. That property is exploited in various holographic studies of, e.g., functional electric potentials, mean inner potentials, and magnetic textures in topical materials. In this contribution we explore two particular aspects of that technique: (I) Its application to two-dimensional materials (2DMs), where their weak scattering power introduce particular Fourier space symmetries, which open up an elegant way to retrieve the projected atomic potentials of the 2DM free from residual aberrations of the imaging system. (II) Its generalization to three-dimensional magnetic vector fields by combining holography with dual tilt axis electron tomography.

(I) Autocorrected off-axis holography of 2DMs

The reduced dimensionality in two-dimensional materials (2DMs) leads to a wealth of unusual properties, which are currently explored for both fundamental and applied sciences. In order to study the crystal structure, edge states, the formation of defects and grain boundaries, or the impact of adsorbates, high-resolution microscopy techniques, such as Transmission Electron Microscopy (TEM), adapted to the specifics of 2DMs (weak scatterer, radiation damage sensitivity), are indispensable. Due to their weak scattering power, most 2DMs behave as weak phase objects (WPOs) in the TEM, i.e., they only slightly modulate the phase of the electron wave transmitting the sample, which is, however, lost when recording the intensity of the electron beam on the detector. Off-axis holography in principle resolves that problem by a reconstruction of amplitude and phase of the electron wave with a gap-free contrast transfer [1].

(II) Three-dimension vector field tomography of magnetic fields in nanomagnetic textures

Three-dimensional (3D) nanomagnetism explores magnetic configurations in confined geometries, where the interplay between exchange, dipolar interaction and anisotropies create a particular rich configuration space. Of particular interest are stable topologically non-trivial solitons referred to as skyrmions, which have been originally conceived as 2D magnetization patterns stabilized by antisymmetric exchange in chiral magnets. Until now crucial details of the full 3D Skyrmion tube (SkT) structure, such as straightness and regularity remain elusive because of a lack of suitable 3D magnetic imaging techniques. In

this contribution, we show how we fill that gap and report on the first 3D reconstruction of a SkT with ten nanometer resolution by employing and adapting vector-field electron tomography (VFET) [2] in the TEM.

Methods

Off-axis electron holography retrieves the phase of the electron beam transmitting the sample from the bending of hologram fringes generated by superimposing the electron beam with an undisturbed reference not scattered by the sample. In case of WPOs such as 2DMs the phases of the Fourier transformed wave are strictly antisymmetric, which can be exploited to detect and correct ubiquitous residual aberrations (e.g., defocus, astigmatism) automatically [1]. We discuss the pertaining algorithms and their behavior, when applied to not strict WPOs (e.g., 2DMs of heavier atoms). In order to reconstruct the full 3D magnetic induction field VFET combines EH with dual-axis tomography to recover the full magnetic flux density \mathbf{B} field [2]. We discuss the whole procedure involving a comprehensive workflow of data processing, including image acquisition, alignment, holographic-tomographic reconstruction and, finally, 3D visualization and analysis. To recover the SkT structure we combined VFET with cryogenic TEM and in-situ application of a rotatable magnetic field to stabilize the skyrmionics magnetic texture in a FeGe needle, while recording the holographic tilt series (Fig. 1) [3].

Results

We use the autocorrected holography technique to reconstruct potentials in multilayered hexagonal Boron Nitride (Fig. 1) and dichalcogenides, such as WSe_2 . We obtain the average electrostatic potential as a function of layer thickness in these materials, delocalized edge states affected by edge reconstructions and defect potentials. The VFET tomogram of the SkTs (Fig. 2) reveals various SkTs that exhibit systematic local deviations from a homogeneous Bloch SkT character (e.g., local losses of axial symmetry, in-plane magnetic flux leaking among neighboring SkTs), a partial collapse of the skyrmion texture at the surface, and a correlated modulation of the SkT axes, amongst others.

References

[1] Kern, F.L. et al., Phys. Rev. Res. 2, 043360 (2020)

[2] D. Wolf et al., Commun. Phys. 2, 87 (2019)

[3] D. Wolf et al., arXiv:2101.12630 (2021)

[4] We acknowledge funding from the European Research Council (ERC) under the European Union's Horizon 2020 research and innovation programme (grant agreement No 715620 and No 856538). We have also received funding from the Deutsche Forschungsgemeinschaft (DFG) under the Schwerpunktprogramm SPP 2137.

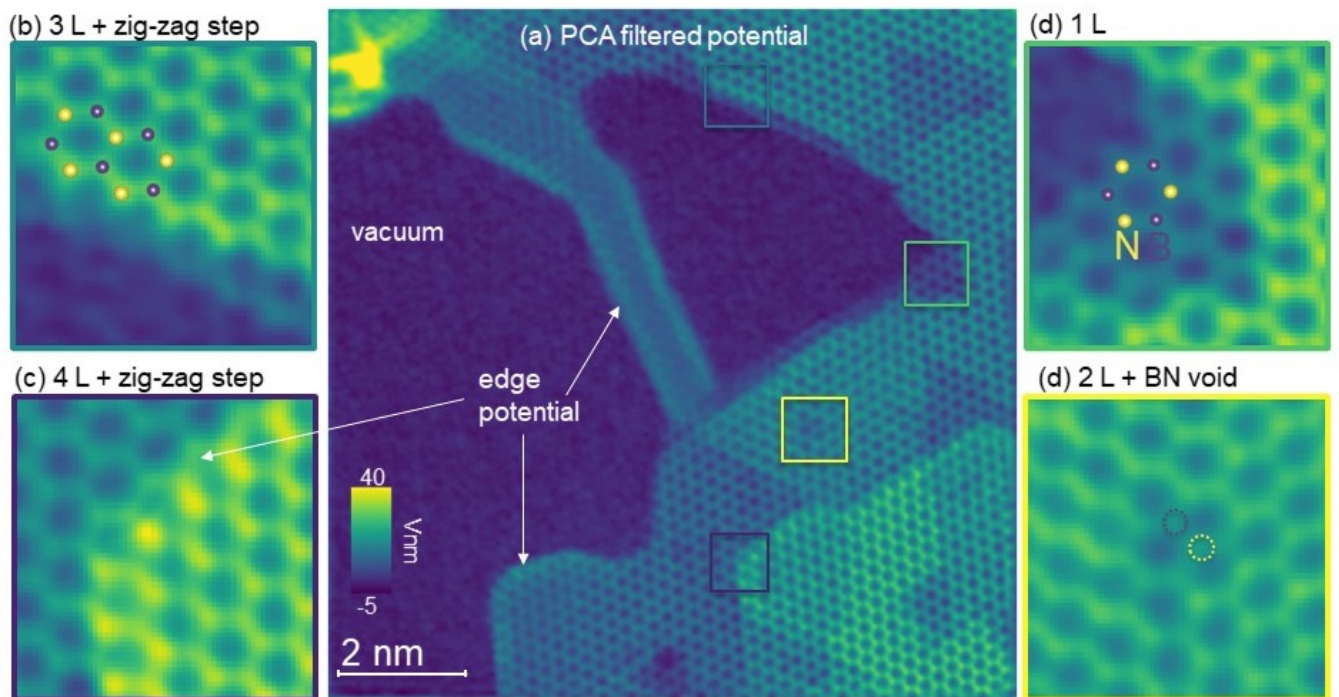


Fig. 1: (a) High-resolution potential analysis in h-BN. Insets: Zig-zag steps comprising two atomic layers (b), (c), a monolayer region (d), and a BN void defect (d). Image adapted from [1].

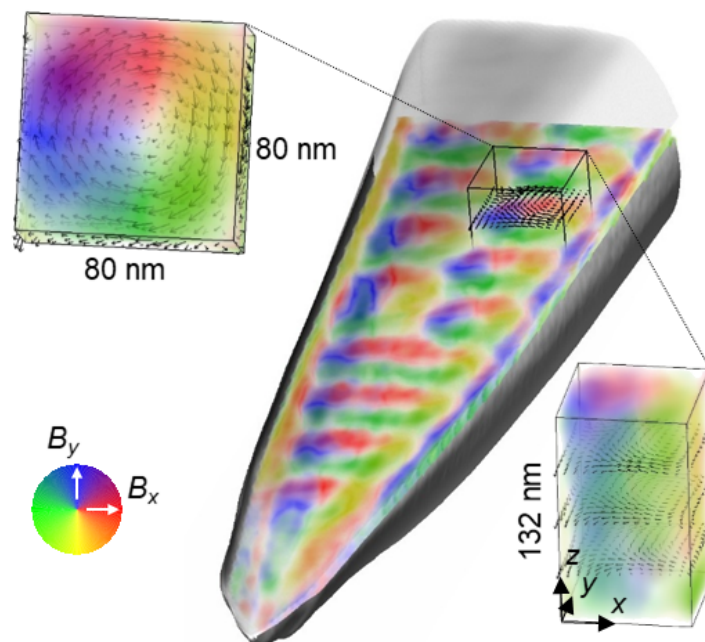


Fig.2: 3D magnetic induction mapping of Bloch skyrmion tubes in FeGe. Volume rendering of the in-plane components B_x , B_y according to the colorwheel and iso-surface of the mean inner potential reconstruction highlighting the FeGe FIB-prepared specimen shape (grey, bottom half only). The magnified views visualize a single skyrmion tube (SKT) in which the three vectors slices plot the 3D spin texture inside the SKT at different z-heights.

Developments for operando electrical measurements in off-axis electron holography

J. Dupuy, M.J. Hÿtch and C. Gatel

CEMES-CNRS, 29 rue Jeanne Marvig, 30155 Toulouse, France.

Electron holography (EH) is an established technique for measuring electric and magnetic fields at the nanoscale. Nevertheless, the studies of weak contributions to the phase shift coming from low charge densities or small magnetic volumes need to improve the signal-to-noise ratio limited by exposure times of a few seconds. Even using a very stable microscope dedicated to interferometric experiments, it is very rare to record holograms for more than 10 s due to remaining instabilities, mainly the fringe and sample drift. A previously explored solution is to acquire image stacks of holograms. Summing the phases of the individual holograms compensates for fringe shifts and numerical reregistration can compensate for specimen drift.

We will show that unlimited acquisition times can be achieved without deterioration of fringe visibility or specimen image definition, by taking active control of the microscope deflectors and stage movements during the acquisition. and without any human intervention. The procedures are robust to low-dose conditions allowing accumulation of signal even when only 5-10 electrons per pixel contribute to individual holograms. The result being a single hologram with an optimized signal over noise ratio which reduces data storage compared with image stacks by several orders of magnitude and allows almost instant appraisal of phase quality [1].

A last part of the talk will concern a short description of the full simulation software of our microscope (Hitachi HF3300C – I2TEM), from the emission of electrons by the cold field emission gun to their detection on the detector plane.

[1] C. Gatel, J. Dupuy, F. Houdellier, M.J. Hÿtch, *Appl. Phys. Lett.* 113, 133102 (2018).

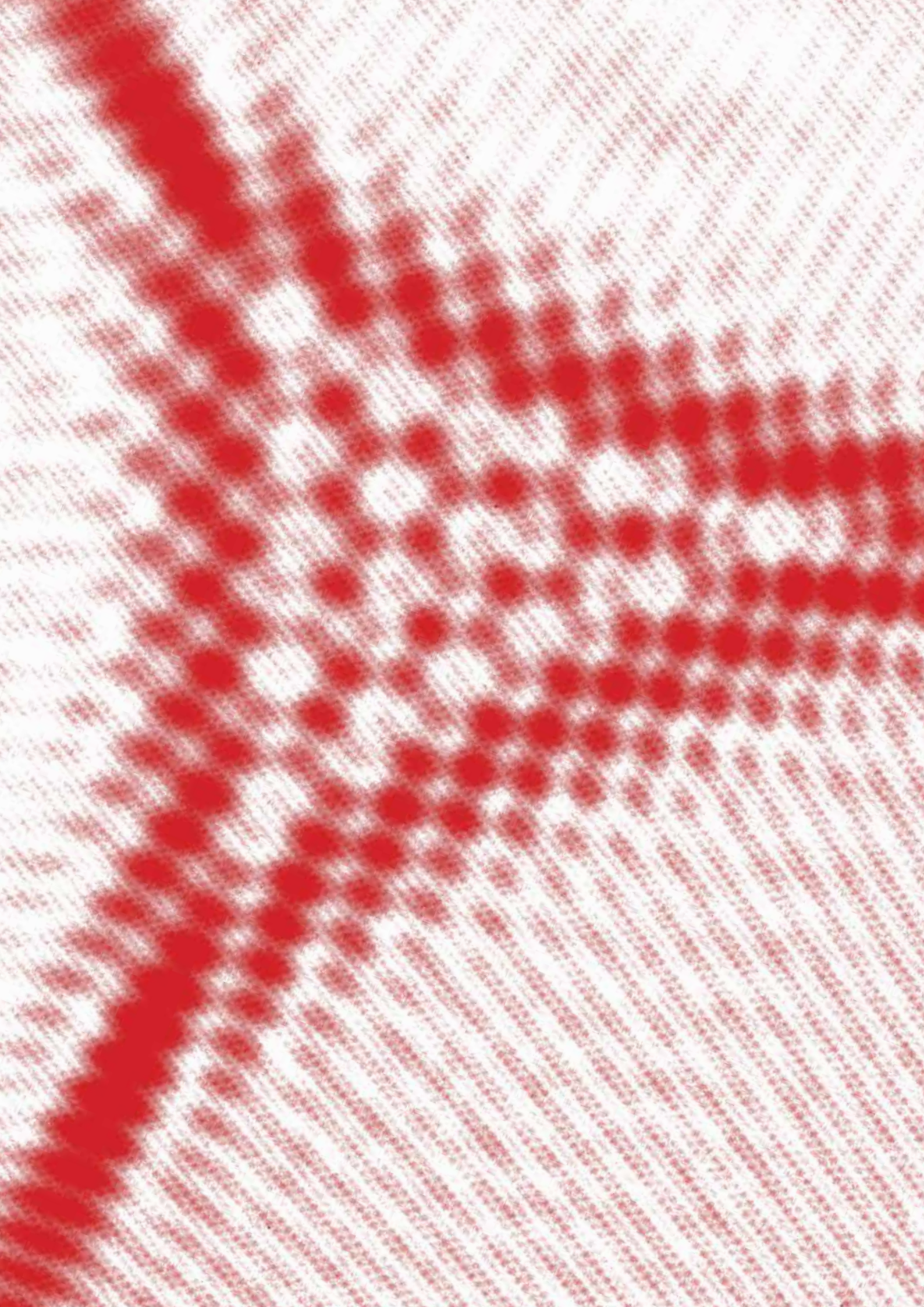
The research leading to these results has received funding from the European Union Horizon 2020 research and innovation program under grant agreement No. 823717 – ESTEEM3. This work has been carried out in the framework of the French national project IODA (ANR-17-CE24-0047) and of the MIMETIS project (No. ANR-10-EQPX-38-01) supported by the French National Research Agency under the "Investissement d'Avenir" program.

Phase anti-matching and other semi-crazy ideas

M. Beleggia

National Centre for Nano Fabrication and Characterization, Technical University of Denmark, DK-2800 Kgs. Lyngby, Denmark

The ability to manipulate locally the electron beam phase brings new tools and perspectives in electron microscopy. One of them is the concept of "functional electron beams", where shaping the illumination allows the electron beam to perform functions either on the object wave, or on the sample, or both, that go very much beyond providing better contrast or dose minimization. Examples are illuminations that match the symmetry of target orbitals, to trigger resonant imaging, non-dispersive beams, or more mundanely one-step nanostructuring of metasurfaces with electron beam lithography. Recent efforts have focused on realizing the analogue of spatial light modulators for electrons, where tunable phasing elements placed at some plane along the imaging system provide us with the opportunity to truly define an arbitrary phase profile that we can add to either the illumination, the object wave or its spatial spectrum. Inspired by dark-field holography, I will discuss the concept of "phase anti-matching", enabled once a tunable pixel-based phase plate becomes available in practice, that allows to capture and separate high- (e.g. atomic structure) and medium-resolution (e.g. electric and magnetic information), to highlight defects, atomic displacements, and field sources at the same time. Amongst the other semi-crazy ideas mentioned in the title, I will discuss whether or not an aberration corrector can be used as a Zernike phase plate, the concept of biprism-less phase reconstruction, interferometric electron beam lithography, and phase-multipole expansion.



Session B:

Ptychography
& 4DSTEM

Ptychography & 4D-STEM: Solutions to a big-data problem

C.T. Koch¹, M. Schloz¹, B. Haas¹, T. Pekin¹, J. Müller¹, G. He¹, S. Shabih¹, and W. Van den Broek²

¹*Humboldt-Universität zu Berlin, Berlin, Germany*

²*Thermo Fisher Scientific, Eindhoven, Netherlands*

Introduction

Far-field ptychography and other ways of interpreting finely sampled (i.e. with probe positions spaced more closely than the probe width) 4D-STEM data have recently become a hot topic, largely due to the availability of fast detectors, fast computers, and advanced reconstruction algorithms. In this presentation a number of results based on the evaluation of zero-loss filtered and unfiltered 4D-STEM data acquired on a direct detector at speeds of up to more than 15,000 fps will be presented. The focus will be on different aspects of ptychography, including ways to minimize the amount of experimental data being recorded while still enabling a high-resolution reconstruction.

Methods

The instrument used for acquiring the data presented in this talk is a Nion HERMES equipped with a Dectris ELA direct detector capable of running at frame rates of up to 18,000 frames per second, when selecting a sub-area of only 130 x 1030 pixels.

While ePIE-type projection algorithms [1] for reconstructing ptychography data are very popular, we employ an explicit derivative - based approach [2,3] for recovering the 2D or 3D object potential from a 4D-STEM data set.

Results

The high speed that modern detectors are capable of enables 4D-STEM data to be acquired such that only very few electrons per pixel are being collected with each frame. This calls for multiple acquisition runs in order to obtain a high signal-to-noise ratio. While such a procedure allows the dose to be spread over a larger time span, the availability of multiple frames per probe position allows non-rigid registration routines, such as implemented in the smartAlign tool [4], to be employed. This way the quality of the acquired data – its resolution and statistics can be improved significantly.

The size of 4D-STEM data sets is often very large, certainly much larger than the amount of information they encode, as demonstrated by the size of reconstructed maps of amplitude and phase or the 3D scattering potential. We have thus explored various ways of compressing the data (e.g. binning and cropping [5], or expansion in an orthonormal basis) and discovered that, depending on the experimental parameters being employed, the data can be reduced to a small fraction of the original size while still being able to recover very

high-resolution maps of the scattering potential. Regularization of the reconstruction helps to allow an even stronger reduction of the data.

Ultimately, we will also discuss new ways of conducting the experiment, such as using specially shaped probes or deviating from the classical raster scan of the electron beam in favor of a more adaptive data acquisition scheme.

References

- [1] A. M. Maiden and J. M. Rodenburg, “An improved ptychographical phase retrieval algorithm for diffractive imaging,” *Ultramicroscopy* **109**, 1256–1262 (2009)
- [2] W. Van den Broek and C.T. Koch, “Method for Retrieval of the Three-Dimensional Object Potential by Inversion of Dynamical Electron Scattering”, *Physical Review Letters* **109**, 24 (2012)
- [3] W. Van den Broek and C.T. Koch, “General framework for quantitative three-dimensional reconstruction from arbitrary detection geometries in TEM”, *Physical Review B* **87**, 18 (2013)
- [4] Colum M. O'Leary, Benedikt Haas, Christoph T. Koch, Peter D. Nellist, Lewys Jones, “Increasing Spatial Fidelity and SNR of 4D-STEM using Multi-frame Data Fusion”, arXiv:2103.03202 [physics.ins-det] (2021)
- [5] M. Schloz, T.C. Pekin, Z. Chen, W. Van den Broek, D.A. Muller, and C.T. Koch, “Overcoming information reduced data and experimentally uncertain parameters in ptychography with regularized optimization”, *Optics Express* **28**, 28306 (2020)

Field mapping by off-axis electron holography and pixelated STEM

V. Boureau¹, Michal Staňo² and D. Cooper³

¹ *Interdisciplinary Center for Electron Microscopy (CIME), EPFL, 1015 Lausanne, Switzerland.*

² *CEITEC BUT, Brno University of Technology, 612 00 Brno, Czech Republic.*

³ *Univ. Grenoble Alpes, CEA, LETI, 38000 Grenoble, France.*

Introduction

Accurate measurements of fields such as elastic strain, electrostatic field or magnetic induction are required by the semiconductor industry for a fine understanding of the devices properties. Over the years, their dimensions become smaller and their control becomes more sensitive to parasitic effects. Electron microscopy therefore faces the challenge of mapping the fields at nanometer scale while maintaining a high sensitivity. Here, off-axis electron holography and pixelated scanning transmission electron microscopy (STEM) are applied to different specimens and some developments on these techniques allowing to fulfill this challenge will be emphasized.

Methods

Off-axis electron holography is a well-established TEM technique for the quantitative mapping of fields. This interferometry technique allows the phase shift induced by the specimen on the electron beam to be mapped. The phase map can then be manipulated to access to different fields. Summation of holograms [1] and π phase-shifting (π PS) [2] have been applied to obtain both strain and electromagnetic potential maps with spatial resolution of about 1 nm while maintaining a useful signal to noise ratio. Pixelated STEM has also been applied to the same specimens. This technique uses a fast camera to record the diffraction patterns for each position of the STEM probe, therefore generating 4D-STEM datasets. Here the fields are calculated by determining the displacements of the beams in the diffraction plane, resulting from the deflection of the electron beam by the specimen. As for holography, analysis of the transmitted beam can be used to retrieve the electromagnetic fields while diffracted beams can be used to access the strain fields.

Results and discussion

Application of the hologram summation and π PS is demonstrated in Fig. 1 [3]. Here the 004 diffracted beam of the specimen was selected with the objective aperture of the microscope to perform dark-field electron holography [4]. It allows the mapping of the out-of-plane strain of an epitaxy of $\text{Si}_{1-x}\text{Ge}_x$ layers with different Ge concentration in a Si matrix. Fig. 1(a) shows two holograms where a phase offset of π has been induced by a precise control of the beam tilt of the microscope. The sum of both holograms can be used to control the accuracy of the phase offset as it ideally shows the intensity of the object wave, while the hologram difference is used

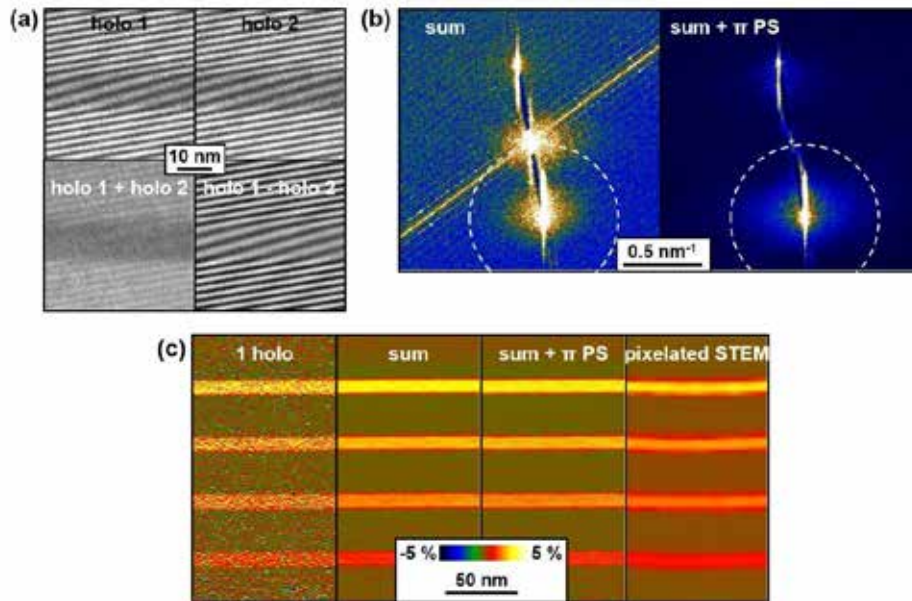


Fig. 1: Out-of-plane strain analysis of $\text{Si}_{1-x}\text{Ge}_x$ layers in a Si matrix. (a) Dark-field holograms, in the vicinity of a SiGe layer, before (holo 1) and after (holo 2) shifting the phase by π . Below, sum and difference of the holograms show the contribution of the center-band and the side-bands, respectively. (b) Fourier transform of the complex images reconstructed from a series of 32 holograms, without (left) and with (right) the use of the π PS method. (c) Strain maps measured by holography using 1 hologram (left), 32 holograms (center-left), 32 holograms plus π PS (center-right); and compared to the measurement obtained with the pixelated STEM technique named PED (right).

to remove this autocorrelation term. The removal of the center-band in the Fourier transform of the hologram is the central idea for π PS. As illustrated in Fig. 1(b), it allows to use a larger numerical aperture during the Fourier reconstruction process of the phase, up to the width of the hologram fringe spacing. Fig. 1(c) shows the strain maps measured by holography using only 1 hologram, a series of 32 holograms and the same series using the π PS method. Fringe spacing of the holograms is 1 nm. Here, the hologram summation increases the strain sensitivity from $8\text{E-}3$ to $1\text{E-}3$, while keeping a spatial resolution of 2.2 nm. The π PS gives access to a spatial resolution of 1.1 nm associated to a sensitivity of $3\text{E-}3$. As a comparison the strain was also measured by precession electron diffraction (PED) [5], a technique that belong to pixelated STEM, as shown in Fig. 1(c). Here a strain sensitivity of $2\text{E-}4$ associated to a spatial resolution of 3 nm is obtained.

An example of magnetic induction field measurement is demonstrated in Fig. 2(a, b). The field of a NiFe ferromagnetic nanowire was measured with a series of holograms and with the pixelated STEM differential phase contrast (PDC) technique [6]. In both measurements, the electrostatic contribution was removed by flipping the specimen in the microscope. Both measurements show a good quantitative agreement with the modelling depicted in Fig. 2(c), as illustrated in the profiles of Fig. 2(d, e). Here again, pixelated STEM shows a better field sensitivity compared with holography, 0.04 T.nm versus 0.09 T.nm, associated with a spatial resolution of 9 nm. However, holography allows to reach higher spatial resolutions at the

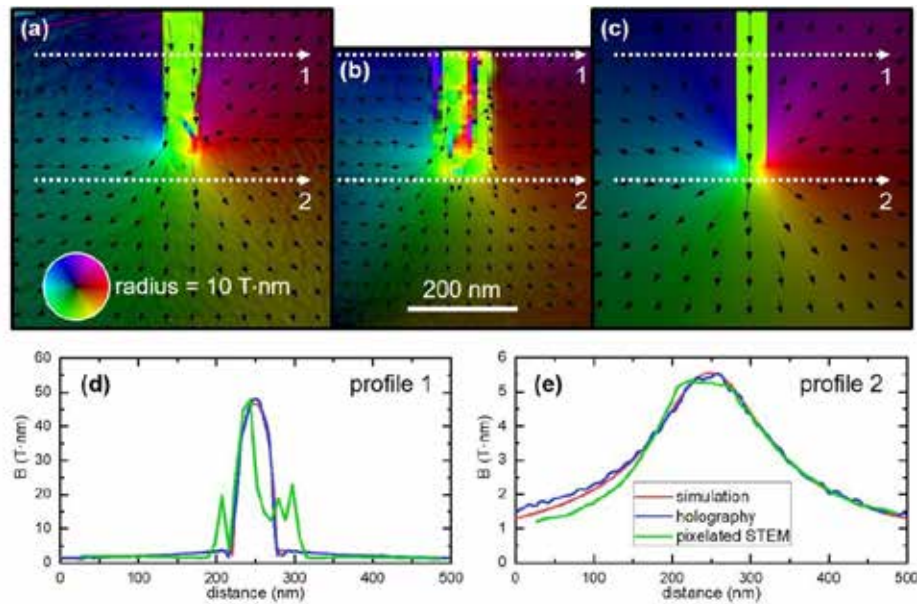


Fig. 2: Maps of the magnetic induction generated by a ferromagnetic NiFe nanowire, (a) measured by holography, (b) measured by pixelated STEM DPC technique and (c) simulated. (d), (e) show profiles of the magnitude of the field, at the location of the dashed arrows.

expense of sensitivity. Also, artifacts from diffraction contrasts and lower spatial resolution prevent pixelated STEM to access the magnetization of the NiFe material.

Advantages and disadvantages of off-axis electron holography and pixelated STEM techniques for measuring fields at the nanoscale will be discussed in the light of the specimen measurements that will be presented. Notably, advantages of using pixelated STEM over off-axis electron holography include the fact that no reference area is needed in the specimen, the field of view is larger and independent from the spatial resolution, the signal to noise ratio is higher as the fields are directly measured thus no derivative of the phase maps are needed. However, artifacts from diffraction contrasts show a strong influence and are difficult to avoid and spatial resolution is usually lower compared to holography.

References

- [1] E. Voelkl & D. Tang, *Ultramicroscopy* **110**, 447–459 (2010).
- [2] Q. Ru, J. Endo, T. Tanji & A. Tonomura, *Applied Physics Letters* **59**, 2372–2374 (1991).
- [3] V. Boureau, R. McLeod, B. Mayall & D. Cooper, *Ultramicroscopy* **193**, 52–63 (2018).
- [4] M. Hÿtch, F. Houdellier, F. Hÿe & E. Snoeck, *Nature* **453**, 1086–1089 (2008).
- [5] J.-L. Rouvière, A. Béch e, Y. Martin, T. Denneulin & D. Cooper, *Applied Physics Letters* **103**, 241913 (2013).
- [6] V. Boureau, M. Staňo, J.-L. Rouvière, J.-C. Toussaint, O. Fruchart & D. Cooper, *Journal of Physics D: Applied Physics* **54**, 085001 (2020).



Session C:

New Magnetic
Measurement Ideas

Advances in the generation and measurement of structured electromagnetic fields in the transmission electron microscope

Amir H. Tavabi¹, Michael Schaaf², Maximillian Kruth¹,
Helmut Soltner², Ulrich Poppe³, Paolo Rosi⁴, Enzo Rotunno⁵,
Alberto Roncaglia⁶, Luca Belsito⁶, Stefano Frabboni^{4,5},
Giulio Pozzi^{1,7}, Gian Carlo Gazzadi⁵, Peng-Han Lu¹, Robert Nijland⁸,
Moumita Ghosh⁸, Peter Tiemeijer⁸, Ebrahim Karimi⁹,
Vincenzo Grillo⁵ and Rafal E. Dunin-Borkowski¹

¹*Ernst Ruska-Centre for Microscopy and Spectroscopy with Electrons and Peter Grünberg Institute, Forschungszentrum Jülich, 52425 Jülich, Germany*

²*Zentralinstitut für Engineering, Elektronik und Analytik, Forschungszentrum Jülich, 52425 Jülich, Germany*

³*Corrected Electron Optical Systems GmbH, Englerstrasse 28, 69126 Heidelberg, Germany*

⁴*Dipartimento FIM, Università di Modena e Reggio Emilia, 41125 Modena, Italy*

⁵*Centro S3, Istituto di Nanoscienze-CNR, 41125 Modena, Italy*

⁶*Istituto per la Microelettronica e i Microsistemi-CNR, 40129 Bologna, Italy*

⁷*Department of Physics and Astronomy, University of Bologna, 40127 Bologna, Italy*

⁸*Thermo Fisher Scientific, PO Box 80066, 5600 KA Eindhoven, Netherlands*

⁹*Department of Physics, University of Ottawa, Ottawa, Ontario K1N 6N5, Canada*

Miniature support-free devices have been proposed for the generation and measurement of structured electromagnetic fields in the transmission electron microscope (TEM) for applications that include high spatial resolution magnetic imaging [1-3]. In this presentation, recent advances in the design, fabrication and implementation of multi-level devices that can be used to characterize magnetic textures in materials and to manipulate electron wave functions in the TEM are reported.

a) Retractable magnetizing unit

A major challenge in the development of magnetic imaging techniques in the TEM, including Lorentz imaging and off-axis electron holography, is the difficulty of applying in-plane magnetic fields to samples *in situ* in the electron microscope, both because of the limited space available for incorporating magnetizing coils and because of the resulting deflection of the electron beam. These difficulties have prevented magnetic switching processes from being studied in the presence of arbitrary applied magnetic field directions. They have also prevented samples from being studied in the presence of applied magnetic fields that maintain their direction with respect to a sample as it is tilted in the electron microscope. Here, we present the concept and design for a retractable magnetizing unit that has five levels of magnetizing coils and can be introduced into a transmission electron microscope using a transfer rod from the opposite side of the microscope column from the conventional goniometer (Fig. 1). The magnetizing unit can

be used to apply external fields to samples that are held in a conventional side-entry specimen holder that allows for cooling, heating and/ or electrical biasing of the sample. It is designed to allow magnetic imaging to be performed with nm spatial resolution in applied magnetic fields of up to 0.5 T that can be applied to the sample in any direction, while correcting for the deflection of the electron beam both above and below the sample.

b) Electrostatic sorter

The component of orbital angular momentum (OAM) in the propagation direction is one of the fundamental quantities of an electron wave function that describes its rotational symmetry and spatial chirality. Here, we demonstrate experimentally an electrostatic sorter device that can be used to analyze the OAM state of an electron beam in a transmission electron microscope [4]. The device achieves post-selection or sorting of OAM states after the interaction of an electron beam with a sample, thereby allowing the study of new material properties such as the magnetic states of atoms. The required electron-optical configuration is achieved by using microelectromechanical systems technology and focused ion beam milling to control the electron phase electrostatically. An OAM resolution of better than $1.3\hbar$ has been achieved in tests on controlled electron vortex beams, with the prospect of reaching an optimal OAM resolution of $1\hbar$ in the near future (Fig. 2).

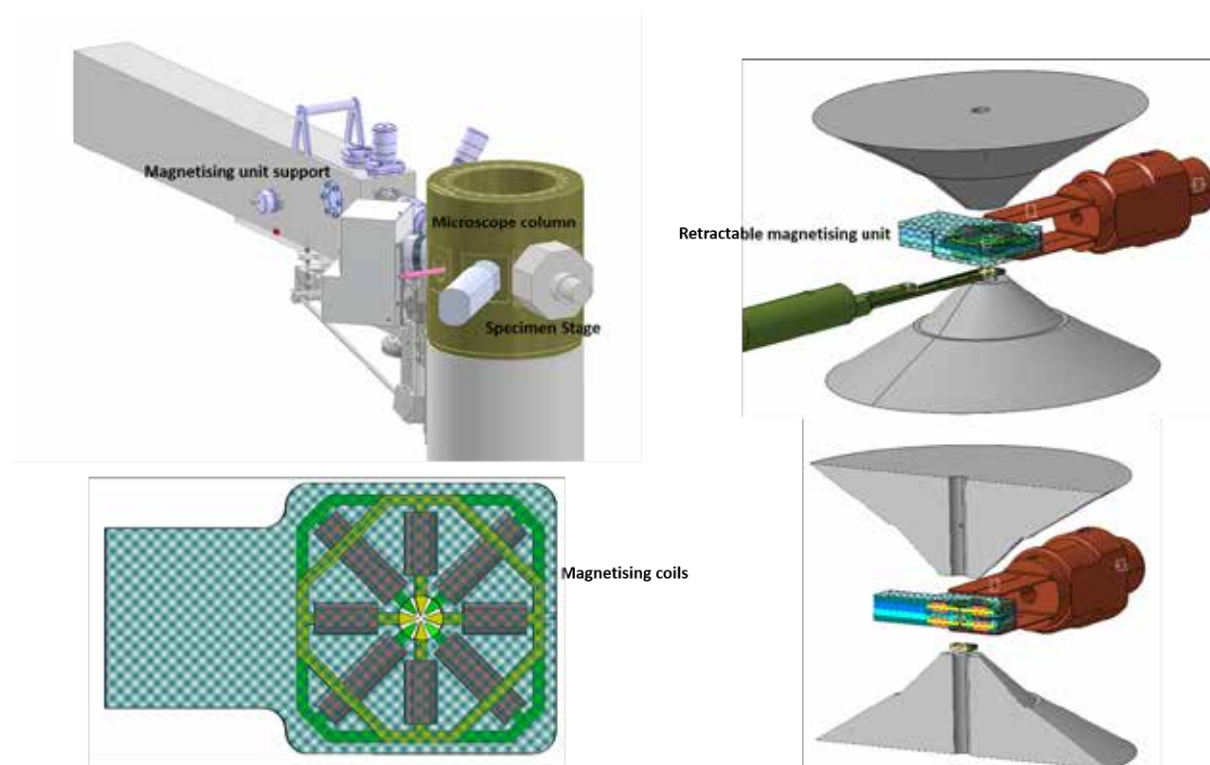


Fig. 1- Design drawings of a retractable magnetizing unit to be installed in the Ernst Ruska-Centre. The magnetizing unit has three levels of coils and can be introduced into the electron microscope using a transfer rod from the opposite sign of the column from the goniometer.

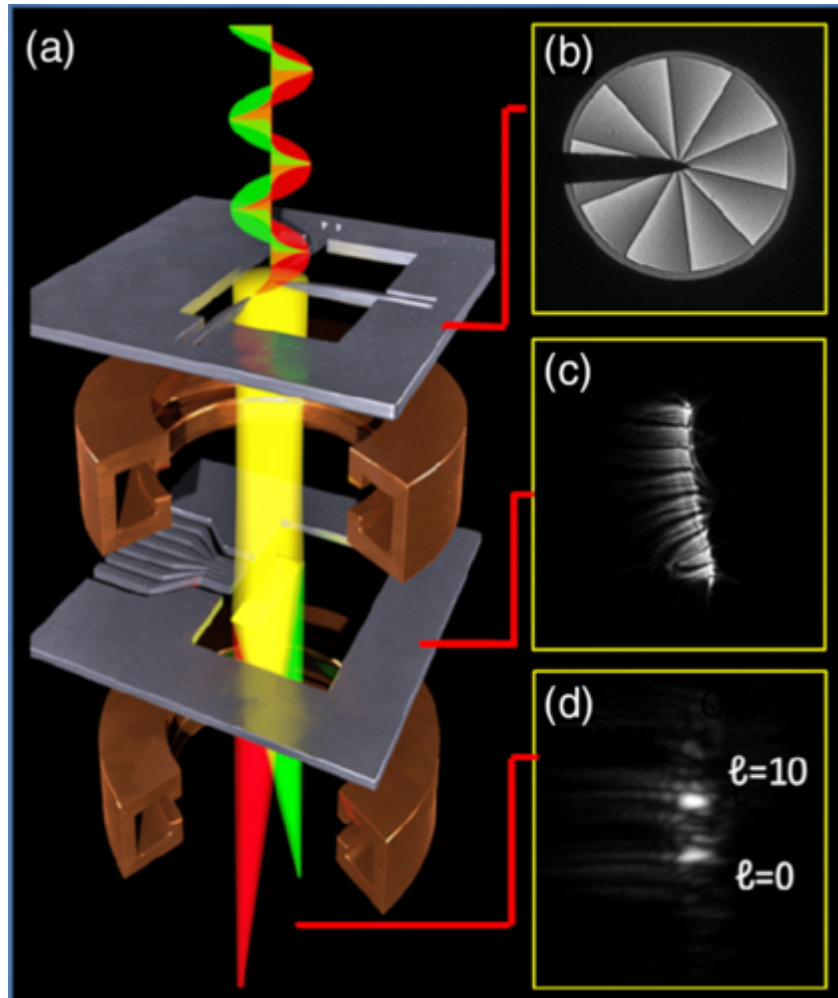


Fig. 2- (a) Schematic drawing of part of an electron microscope column that contains a sorter device. (b)-(d) Experimental images of the evolution of the electron wave function for a nominal superposition of $|\ell = 10\rangle$ and $|\ell = 0\rangle$, showing (b) generation, (c) conformal transformation to polar co-ordinates and (d) transformation into an orbital angular momentum spectrum.

References

- [1] US Patent 10,607,804
- [2] US Patent 10,276,345
- [3] PT 1.2846 G IT
- [4] A. H. Tavabi et. al, Phys. Rev. Lett. **126**, 094802, 2021

Imaging of complex magnetic textures with particle-like properties

Nikolai. S. Kiselev

¹*Institute for Advanced Simulation and Peter Grünberg Institute,
Forschungszentrum Jülich, Germany*

Off-axis electron holography is a very powerful tool for imaging magnetic textures in confined geometry samples [1] not accessible by standard Lorentz TEM. It provides quantitative data on the strength of the projected in-plane component of the induction field produced by the sample. We use off-axis electron holography for imaging complex magnetic textures with particle-like properties (solitons) such as chiral magnetic skyrmions [2-3], skyrmion bags [4-5], chiral bobbars [6-7], and skyrmions braids [8]. These magnetic textures can be formed in isotropic chiral magnetic crystals, e.g., B20-type crystals of Si- and Ge-based alloys such as FeGe, MnSi, CoFeSi, etc. The stability of such magnetic textures typically requires the external magnetic field and can be explained by the competition between Heisenberg exchange and chiral Dzyaloshinskii-Moriya interaction. Besides that, quantitative agreement between experimentally observed phenomena and theoretical modeling requires taking into account the effect of demagnetizing fields. We combine the advanced computational methods in micromagnetic model of chiral magnets and state-of-the-art off-axis electron holography technique to show an excellent quantitative agreement between theory and experimental observation. To find theoretically the stable configurations of skyrmions bags, chiral bobber and skyrmions braids we perform numerical energy minimization of micromagnetic functional by means of conjugate gradient method implemented for massively parallel computations of modern GPU. The later allows to perform energy minimization of the functional including demagnetizing fields and real time visualization of theoretical Lorentz TEM images and electron phase shift map expected in electron holography experiment.

In my presentation, first, I will briefly introduce the theory of magnetic solitons in isotropic chiral magnets. Then, I will focus on the overview of the most recent progress in imaging of these objects with Lorentz TEM and off-axis electron holography in FeGe plates.

- [1] C. Jin et al., Nat. Commun. **8**, 15569 (2017).
- [2] K. Shibata et al., Phys. Rev. Lett. **118**, 087202 (2017).
- [3] A. Kovács et al., Appl. Phys. Lett. **111**, 192410 (2017).
- [4] F. N. Rybakov and N. S. Kiselev, Phys. Rev. B **99**, 064437 (2019).
- [5] D. Foster et al., Nat. Phys. **15**, 655 (2019).
- [6] F. N. Rybakov et al., Phys. Rev. Lett. **115**, 117201 (2015).
- [7] F. Zheng et al., Nat. Nanotech. **13**, 451(2018).
- [8] F. Zheng et al., arXiv:2104.01682

ULTRAFast SPECTROSCOPY

from fundamental concepts to applications in magnetism

Theo Rasing

Radboud University, Institute for Molecules and Materials, Heijendaalseweg 135,
6525AJ Nijmegen, the Netherlands

Femtosecond laser pulses are among the fastest stimuli in (condensed matter) physics and allow to interrogate and study matter at the fundamental time scales of electron-electron, electron-phonon and spin-lattice relaxation, in the range between a few femto to hundreds of picoseconds. Typical experiments are of a pump-probe fashion in which a strong laser pulse acts as a pump to bring the system of interest out of equilibrium, where after a well-defined delay time a much weaker probe pulse measures the state of the system at that time. By varying the delay between pump and probe, the dynamics of the time evolution of the system can be probed. Standard pump-probe experiments use visible laser pulses for pump and probe, in which primarily the electronic system is excited and probe. By extending this to longer (infrared) wavelengths (or THz frequencies), fundamental excitations like phonons or magnons can directly be excited and probed. On the other hand, recent developments in X-ray Free Electron Lasers allow to extend these experiments to the X-ray regime, thereby combining the shortest length with the shortest time scales.

In this talk the fundamentals and recent developments of pump-probe spectroscopy will be introduced and illustrated with a number of exemplary examples in ultrafast magnetization dynamics that demonstrate the power (and shortcomings) of the various techniques.



Session D:

Phase and field
holography

Off-axis electron holography and Lorentz microscopy of magnetic skyrmion bubbles in multilayers and van der Waals materials

T. Denneulin¹, J. Caron¹, A.H. Tavabi¹, A. Kovács¹
and R.E. Dunin-Borkowski¹

¹*Ernst Ruska-Centre for Microscopy and Spectroscopy with Electrons and Peter Grünberg Institute, Forschungszentrum Jülich, 52425 Jülich, Germany.*

Introduction

Skyrmions are whirl-like magnetic textures that are elementary building blocks of possible future low-power storage and logic devices [1]. They were first observed at low temperature in B20-type compounds [2] and were subsequently found in various magnetic systems, including bulk crystals and heterostructures [3]. In this presentation, we focus on skyrmions in multilayers and van der Waals crystals.

Thin films of heavy metals and ferromagnets are interesting candidates for applications because they can host skyrmions at room temperature and can be deposited by sputtering, which is used extensively in industry. Their broken inversion symmetry and the strong Dzyaloshinskii–Moriya interaction (DMI) at their interfaces favor the formation of Néel-type skyrmions [4]. Néel-type skyrmions in out-plane-magnetized layers can be observed using Lorentz transmission electron microscopy by tilting the sample with respect to the incident electron beam direction [5]. However, the magnetic contrast is weak, both because only a small component of the magnetic field contributes to it and because of superimposed diffraction contrast from the polycrystalline grain structure. In this work, we use Fresnel defocus imaging and off-axis electron holography to study Néel-type skyrmions in multilayers [6]. We will discuss how to optimize the magnetic signal-to-noise ratio.

Layered van der Waals (vdW) crystals are considered to be ideal materials for two-dimensional spintronic applications, such as atomically-thin and flexible magneto-optic and magnetoelectric devices [7], motivating research on vdW materials that are long-range-ferromagnetically-ordered at room temperature. Here, we study the vdW materials Fe₃GeTe₂ and Fe₅GeTe₂, which exhibit perpendicular magnetocrystalline anisotropy and have relatively high Curie temperatures of ~200 and ~300 K, respectively, in bulk crystals [8,9].

Methods

The nominal composition of the investigated multilayer sample is Ta(3) / Pt(1.5) / [Pt(1.5) / Co(0.3) / Ni_{0.8}Fe_{0.2}(0.9)] ×5 / Ru(0.5) / Pt(2), where the numbers between parentheses correspond to thicknesses of the layers in nm and ×5 represents the number of repetitions. The stack was deposited onto a 15-nm-thick SiN membrane using DC magnetron sputtering.

Single crystals of Fe_5GeTe_2 were synthesized using chemical vapor transport. Cross-sectional and plan-view lamellae were prepared using focused Ga^+ ion beam sputtering in an FEI Helios workstation.

Scanning transmission electron microscopy (STEM) and energy-dispersive X-ray spectroscopy (EDX) were carried out at 200 kV using an FEI Titan TEM equipped with a Schottky field emission gun, a CEOS probe aberration corrector, a high-angle annular dark-field (HAADF) detector and a Super-X EDX detection system.

Off-axis electron holography and Fresnel defocus imaging were carried using an FEI Titan TEM equipped with a Schottky field emission gun, a CEOS image aberration corrector and a $4\text{k} \times 4\text{k}$ Gatan K2-IS direct electron detector. The microscope was operated at 300 kV in magnetic-field-free conditions (Lorentz mode) by using the first transfer lens of the aberration corrector as the primary imaging lens. The conventional microscope objective lens was used to apply pre-calibrated magnetic fields to the sample.

Results

Figure 1(a) shows an image and compositional maps of a cross-sectional sample of the $(\text{Pt}/\text{Co}/\text{NiFe}) \times 5$ multilayer. The total thickness of the stack is 20.5 nm, including only 6 nm of ferromagnetic material. Figure 1(b) shows an electron optical phase image of a plan-view sample recorded at room temperature at a sample tilt angle of 25° in an externally applied magnetic field of 23 mT. Non-magnetic contributions to the phase have been removed by subtracting a second phase recorded after saturating the sample magnetically. Three skyrmion bubbles can be observed, as a result of the projection of the out-of-plane component of the magnetic field into the image plane. Figure 1(c) shows a corresponding color-coded magnetic induction map. The magnetic field inside the skyrmion (yellow region) is oriented in the opposite direction to that in the outside domain (purple region). The stray field rotates around the skyrmion's core.

Figure 1(d) shows an atomic-resolution HAADF STEM image of a cross-sectional sample of Fe_5GeTe_2 . Each vdW layer comprises two planes of Te (brightest columns), which are separated by Fe and Ge columns. Figures 1(e) and 1(f) show an electron optical phase image of a 100-150 nm thick plan-view sample of Fe_5GeTe_2 recorded at 200 K and a corresponding color-coded magnetic induction map. Bloch-type skyrmion bubbles with two possible helicities (the rotation of the magnetization at the domain wall can be clockwise or counter-clockwise), as well as type-II bubbles, can be observed.

Discussion

Skyrmion bubbles were observed at room temperature in a multilayer sample using off-axis electron holography. Although not shown in the figures, no magnetic contrast was observed at 0° , confirming that the magnetic texture of the domain wall is Néel-type [5]. The Fe_5GeTe_2 sample showed type-I bubbles with both chiralities and type-II bubbles at 200 K. The random chirality of the bubbles indicates that they are stabilized by dipolar interactions rather than DMI. The Curie temperature of the sample was found to be ~ 250 K.

Future possible experiments include current-induced skyrmion motion and three-dimensional investigations of skyrmion texture. 3D reconstructions of Néel-type skyrmions are more challenging than for Bloch-type skyrmions because of a lack of information at the domain wall.

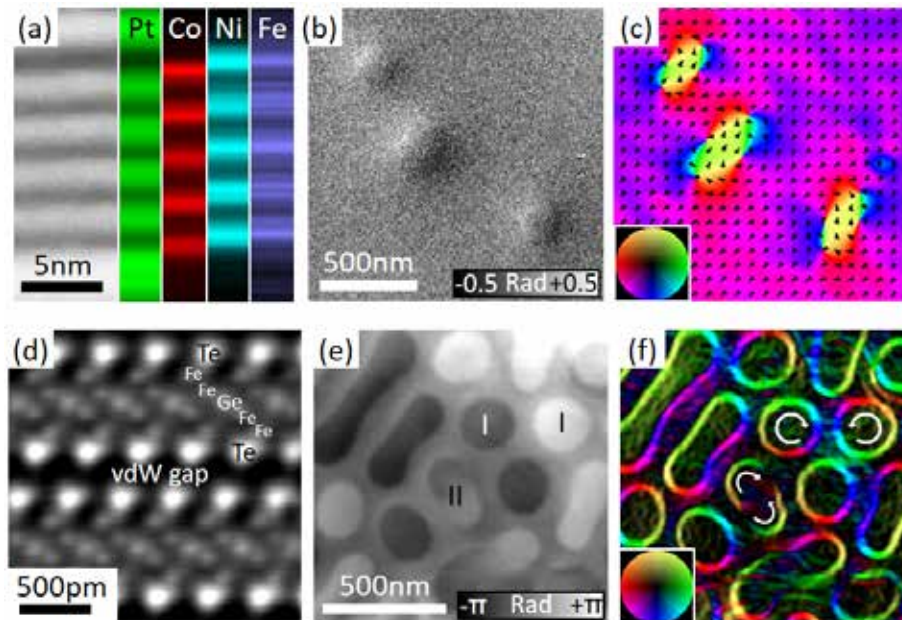
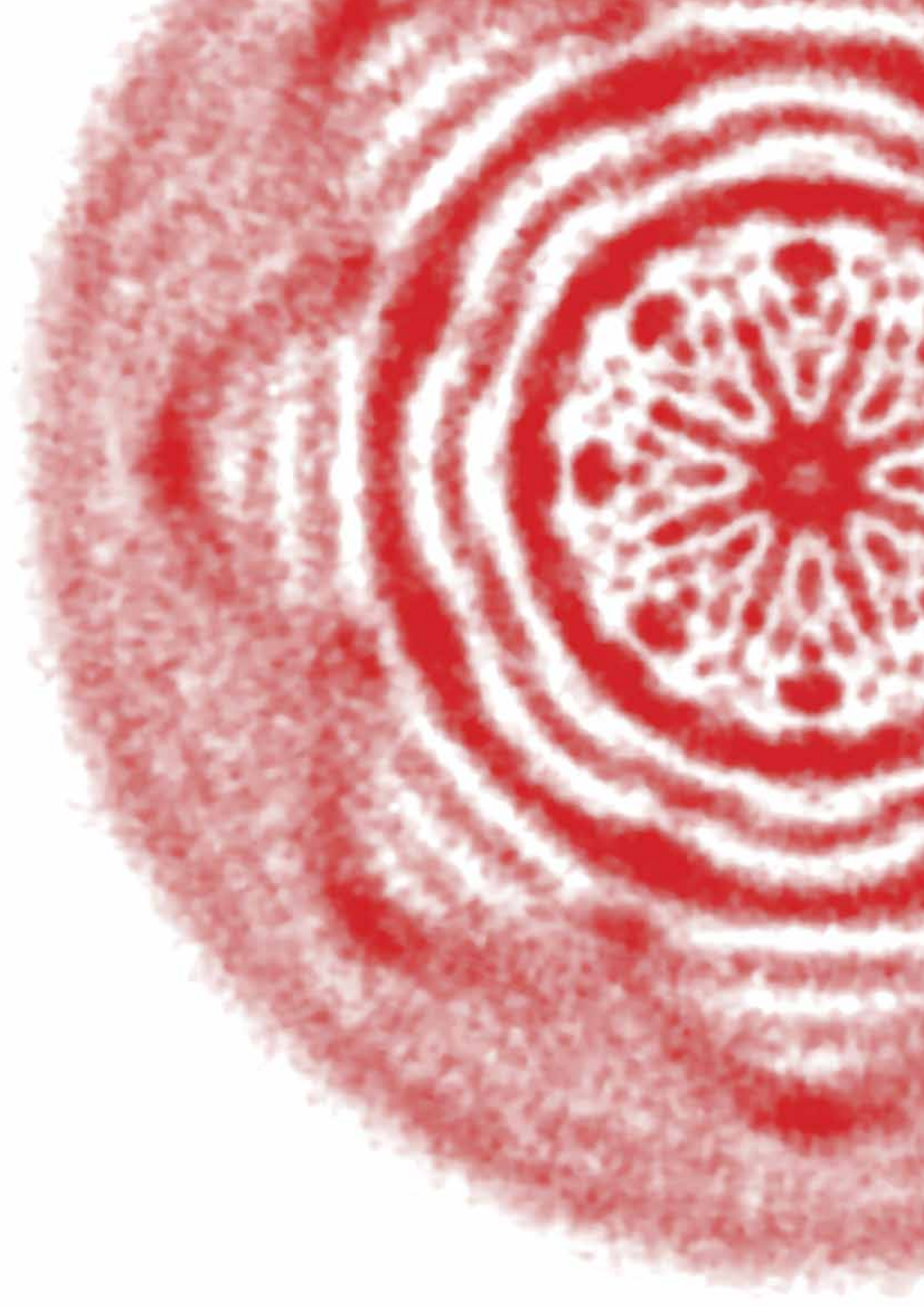


Fig. 1 (a) HAADF STEM image of a cross-sectional sample of a (Pt/Co/NiFe) \times 5 multilayer and EDX compositional maps averaged in the horizontal direction. (b) Electron optical phase image of a plan-view sample of a (Pt/Co/NiFe) \times 5 multilayer recorded at room temperature at a sample tilt angle of 25° in the presence of an externally applied magnetic field of 23 mT. (c) Corresponding color-coded magnetic induction map. (d) HAADF STEM image of a cross-sectional sample of single crystalline Fe₅GeTe₂. (e) Electron optical phase image of a plan-view sample of Fe₅GeTe₂ recorded at 200 K at a sample tilt angle of 0° in zero applied magnetic field. (f) Corresponding color-coded magnetic induction map.

References

- [1] A. Fert et al., *Nature Review Materials* **2**, 17031 (2017)
- [2] S. Mühlbauer et al., *Science* **323**, 915-919 (2009)
- [3] K. Everschor-Sitte et al., *Journal of Applied Physics* **124**, 240901 (2018)
- [4] C. Moreau-Luchaire et al., *Nature Nanotechnology* **11**, 444-448 (2016)
- [5] S. D. Pollard et al., *Nature Communications* **8**, 14761 (2017)
- [6] T. Denneulin et al., *Ultramicroscopy* **220**, 113155 (2021)
- [7] C. Gong and X. Zhang, *Science* **363**, eaav4450 (2019)
- [8] Y. Deng et al., *Nature* **563**, 94-99 (2018)
- [9] A. F. May et al., *ACS Nano* **13**, 4436–4442 (2019)

The authors acknowledge funding from the DARPA TEE program grant MIPR# HR0011831554 and the European Union’s Horizon 2020 Research and Innovation Programme under grant agreement 856538 (project “3D MAGIC”).



Session E:

Ptychography
& 4D-STEM

Segmented- and pixelated-detector differential phase contrast imaging of the iron-rhodium magnetostructural transition

T. Almeida¹, R. Temple², J. Massey², D. McGrouther³, L. Molina⁴, A. Chirkova⁴, K. Skokov⁴, C. H. Marrows² and S. McVitie³

¹Université Grenoble Alpes, CEA, Leti, F-38000 Grenoble, France

²School of Physics and Astronomy, University of Leeds, LS2 9JT, UK

³School of Physics and Astronomy, University of Glasgow, G12 8QQ, UK.

Department of Materials, Technische Universität Darmstadt, 64287, Germany

Introduction

The ordered α' alloy of iron-rhodium ($\text{Fe}_{48}\text{Rh}_{52}$ to $\text{Fe}_{56}\text{Rh}_{44}$) has attracted considerable attention due to its magnetostructural transition from its antiferromagnetic (AF) to ferromagnetic (FM) phase¹. α' -FeRh undergoes a first-order phase transition from its room-temperature AF state to FM between ~ 350 to 380 K, and can hence present phase AF/FM co-existence, separated by phase-boundary (PB) domain walls (DWs). Controlled nucleation and movement of these PBs is considered very desirable for potential use in magnetic data storage applications². Previous studies have shown that the PBs can be created and driven in FeRh films by combining heating with differential gradients of chemical doping^{3,4}, where dopants of iridium and palladium have been shown to decrease and increase the transition temperature, respectively³. However, our knowledge of the dynamic behaviour of PBs in FeRh is often indirect, limited to bulk magnetic measurements or low magnification imaging, i.e. Kerr microscopy. In order to fully understand the magnetostructural transition and dynamic motion of PBs, it is necessary to examine the effect of temperature directly. The scanning transmission electron microscopy (STEM) technique of differential phase contrast (DPC) imaging permits nanometre-scale imaging of magnetisation within nanostructured thin films as a function of temperature. Here, the use DPC imaging acquired with both a conventional segmented- and pixelated-detector to examine the magnetic domain evolution and heat-induced PB motion in cross-sectional FeRh thin films is presented.

Methods

Uniform and Ir / Pd gradient-doped thin films of ordered α' -FeRh alloy were grown epitaxially on clean (001) MgO substrates by conventional DC magnetron sputter co-deposition, as described previously⁵. Cross-sectional TEM samples were prepared from bulk substrates and transferred onto in situ heating (DENSsolution WildfireTM) TEM electronic (e-) chips by focused ion beam methods⁶. Conventional and high-resolution STEM imaging of the FeRh films and substrates was performed using a JEOL ARM cFEG instrument at 200kV, whilst energy dispersive X-ray (EDX) spectroscopy provided chemical analysis. In order to recover the ordered α' FeRh structure after FIB preparation, the cross-sectional samples were annealed in situ in the TEM at 650°C for 1 hour using the DENSsolution e-chips. The magnetic

structure of the films is visualised using DPC imaging under low-magnetic field conditions and in situ heating up to 200°C provides direct access to the dynamics of the FM domain nucleation /evolution within the uniform FeRh films. In addition, systematic PB motion in the gradient-doped FeRh cross-sections is induced as a function of temperature.

Results and Discussion

Figure 1 presents a cross-section of a uniform FeRh thin film, providing information on its thickness, localized structure and interface with the MgO substrate⁶, as well as its magnetization. The dark-field (DF) STEM image of Fig. 1a reveals the FeRh film to be grown with a uniform thickness of ~ 52 nm, whilst the high-resolution STEM image of Fig. 1b presents the interface between the single crystalline FeRh and MgO substrate, revealing their well-matched orientation and confirming the epitaxial growth of the deposited FeRh. The DPC image of Fig. 1c reveals the growth of a green magnetic domain (~ 200 nm wide, right-hand side) at the FeRh / MgO interface at 93°C. As the temperature is increased to 200°C, a large magnetic domain (red) with opposite direction of magnetism is observed to form on the left hand-side of the FeRh thin film (Fig. 1d), where a small domain (blue, arrowed) considered to be a transverse DW is seen to separate the larger domains (green and red). Hence, this localized analysis provides fundamental insight into domain evolution during the AF to FM transition⁷.

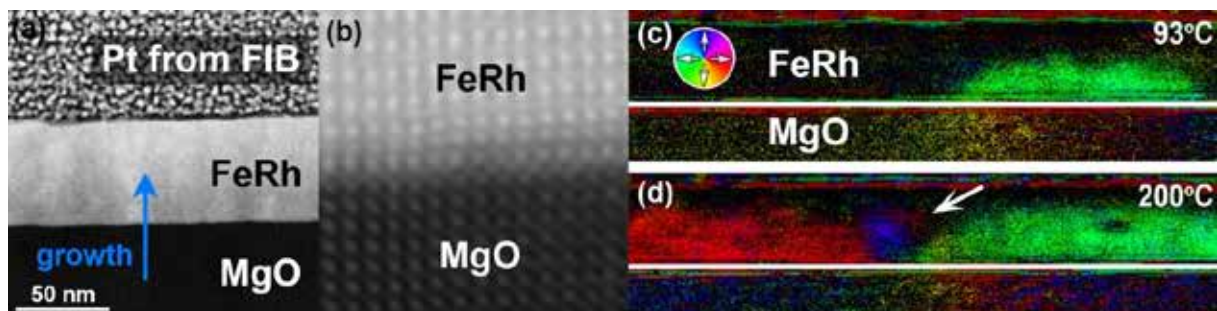


Figure 1. (a) DF STEM image of a FeRh thin film grown epitaxially on the MgO substrate. (b) High resolution STEM image showing the epitaxially grown FeRh and its interface with the MgO substrate. (c,d) DPC imaging of a uniform FeRh film cross section showing: (c) growth of a FM domain (green) at the FeRh / MgO substrate at 93°C; and (d) green and red FM domains at 200 °C separated by a transverse DW (blue, arrowed). The direction of magnetization is depicted in the color wheel (inset).

Figure 2 presents a cross-section of the Ir / Pd gradient-doped FeRh thin film, providing information on its chemical distribution and magnetism as a function of temperature. The EDX chemical maps (Fig. 2a) display the elemental distribution of palladium and iridium dopants within the FeRh thin film. The palladium dopant content is uniformly distributed along the cross-section, whilst the iridium dopant exhibits a gradient from high (top) to low (bottom) content. The DPC images of Fig. 2b presents the AF / FM PB motion as a function of increasing temperature. At 50°C, no magnetic signal is evident in the top Ir-rich side of FeRh thin film and hence considered AF, distinct from the FM bottom side (green), suggesting they are separated by an AF/FM PB. As temperature is increased, the green FM domain migrates upwards, inducing upward PB motion, until the FeRh film is fully FM at 200°C. Fig. 2c displays the AF /

FM PB motion as a function of decreasing temperature from 150°C, where it is in a fully-FM state. As the FeRh thin film is cooled to 20°C, the very top layer of the FeRh becomes AF, and the PB progressively migrates downwards towards the center. Hence, this study shows that PB motion can be controlled systematically using temperature and Ir-gradient doping.

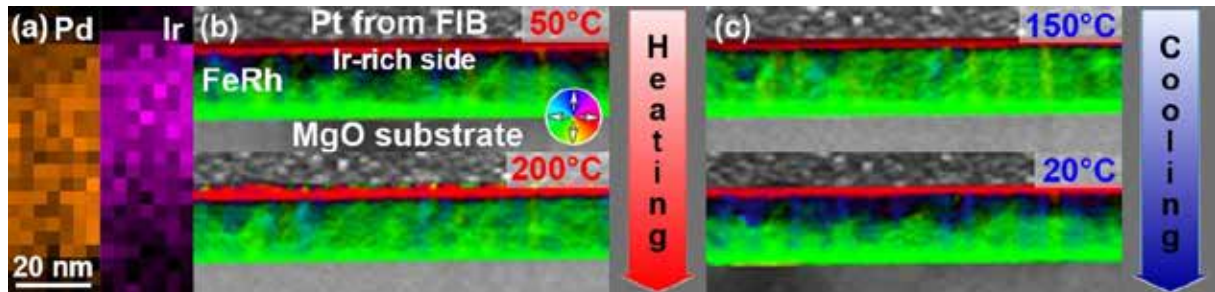


Figure 2. (a) EDX chemical maps displaying the elemental distribution of palladium (orange) and iridium (pink) content, revealing the high (top) to low (bottom) gradient in iridium. (b) DPC imaging of the Ir/Pd gradient-doped FeRh film as a function of increasing temperature, displaying the upward PB motion to the Ir-rich side. The direction of magnetization is depicted in the colour wheel (inset). (c) DPC imaging as a function of decreasing temperature, displaying the downward PB motion.

Figure 3 presents a planar TEM sample fabricated from a bulk FeRh crystal. The DPC images reconstructed from pixelated DPC data revealed the domain growth evolution with temperature through phase correlation / edge detection of the central disk. This allowed the isolation of the magnetic domains, separate from the effects of diffraction contrast.

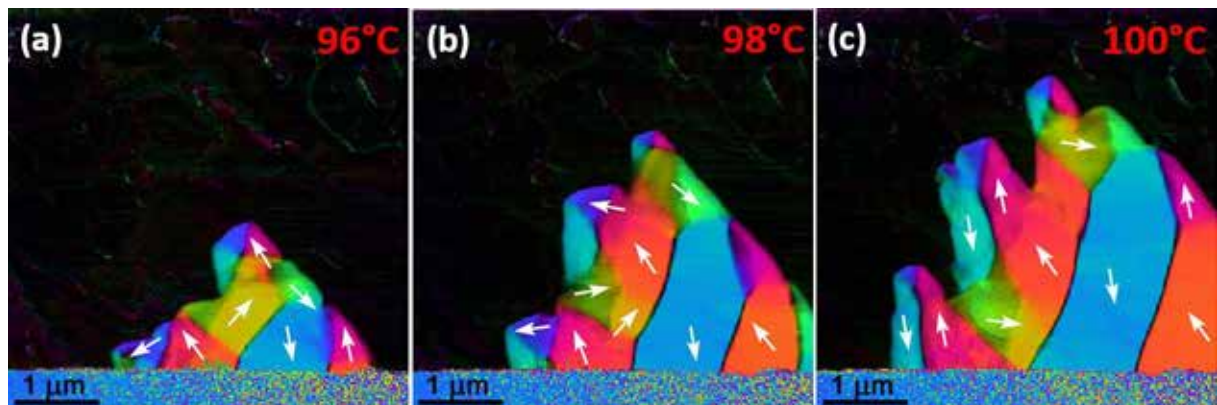


Figure 3. Pixelated DPC images acquired from a FeRh sample at (a) 96°C; (b) 98°C; and (c) 100°C.

References

- [1] L H Lewis et al., *J. Phys. D: Appl. Phys.* **49**, 323002 (2016).
- [2] X. Marti et al., *Nature Mat.* **13**, 367-374, (2014).
- [3] C. Le Graët et al., *APL Mater.* **3**, 041802 (2015).
- [4] C. Le Graët et al., *J. Vis. Exp.* **80**, e50603 (2013).
- [5] T. P. Almeida et al., *J. Phys. Conf. Ser.* **903**, 012022 (2017).
- [6] T. P. Almeida et al. *Sci. Rep.* **7**, 17835 (2017).
- [7] T. P. Almeida et al. *Phys. Rev. Materials* **4**, 034410 (2020).

Phase Retrieval by Electron Ptychography

David. A. Muller^{1,2}

1. School of Applied and Engineering Physics, Cornell University, Ithaca, NY, USA
2. Kavli Institute at Cornell for Nanoscale Science

Introduction

The past three decades have seen the rapid development and maturation of aberration-corrected electron lenses [1,2]. With recent advances in detector technology and reconstruction algorithms, the resolution of the electron microscope is now limited by the dose to the sample, and thermal vibrations of the atoms themselves [3]. By recording the full position-momentum phase space, and using ptychographic algorithms to solve the multiple-scattering inverse problem in thick samples, we have been able to improve the dose efficiency of the imaging beyond all other electron microscopy methods, and equally important, obtain the highest resolution images ever recorded. The linearity of the recovered phase signal makes it possible to locate individual dopant atoms in 3D.

Proper treatments of the probe coherence are essential for robust reconstructions, and for us, using a mixed-state approach has helped considerably and made it possible for use to work with more complicated incident wavepackets [4]. These approaches have also allowed us to image strain in devices, magnetic fields in sub-nm thick layers, as well as the internal structures of both magnetic and ferroelectric vortices, skyrmions and merons, including their singular points that are critical for accurately describing the topological properties of these field textures.

Looking forward, the use of phase plates and shaping coherent beams for increased signal diversity look like promising methods to improve the quality of ptychographic phase reconstructions, especially at low doses [5].

Methods

Ptychography uses scanning diffraction and 4D-STEM datasets to iteratively reconstruct the electrostatic potential [6–8] and has reached a resolution of 39 pm in thin 2D materials [9] [5]. However, conventional ptychography (single-slice) assumes that the exit-surface wave function can be expressed as a multiplication of the incident probe and a single complex transmission function whose phase represents the sample projected potential. This approximation usually fails for samples thicker than a few nanometers in the presence of strong multiple scattering. For thick samples, attempts at phase retrieval from both multi-slice electron ptychography [10,11] and Bloch wave based scattering matrix [12] approaches have been reported. However, to date, none of the experimental demonstrations have been widely adopted due to limited resolution or image quality.

Here, we demonstrate a robust experimental realization of inversion of the multiple scattering using a regularized implementation of multislice electron ptychography [3]. This approach provides ultra-high-resolution reconstructions for samples hundreds of Angstroms thick (Figure 1(a)). More importantly, the contrast maintains a linear dependence on thickness over a wide thickness range. The linear phase-contrast can also greatly widen the applicable sample thickness and makes it possible to obtain three-dimensional structural information including the locations of single dopant and interstitial atoms (Figure 2).

Results

The potential reconstructed from multislice ptychography from an experimental dataset acquired from a 21-nm-thick PrScO_3 sample (Figure 1a), similar to that from a simulated dataset shows only a slight additional blurring compared to the potential at 300 K (Figure 1c). The diffractogram of the phase image shows an isotropic information transfer up to 4.39 \AA^{-1} , corresponding to 23 pm in real space. Quantitative analysis of the atomic column width reveals that the blurring from the instrument is smaller than 20 pm, which is smaller than the intrinsic broadening from thermal fluctuations. The method also allows for direct measurements of Debye-Waller factors of atoms near defects or interfaces.

Ptychography is also valuable for magnetic imaging, where the need for field-free conditions limits the spatial resolution achievable by the microscope objective lens. Fig 3 shows how Lorentz electron ptychography has allowed us to achieve magnetic field imaging beyond the diffraction limit imposed by the optics of the electron microscope. The improved sensitivity and resolution allows us to directly resolve the internal fine structures of magnetic skyrmions near the skyrmion cores, boundaries and dislocations in single crystal FeGe.

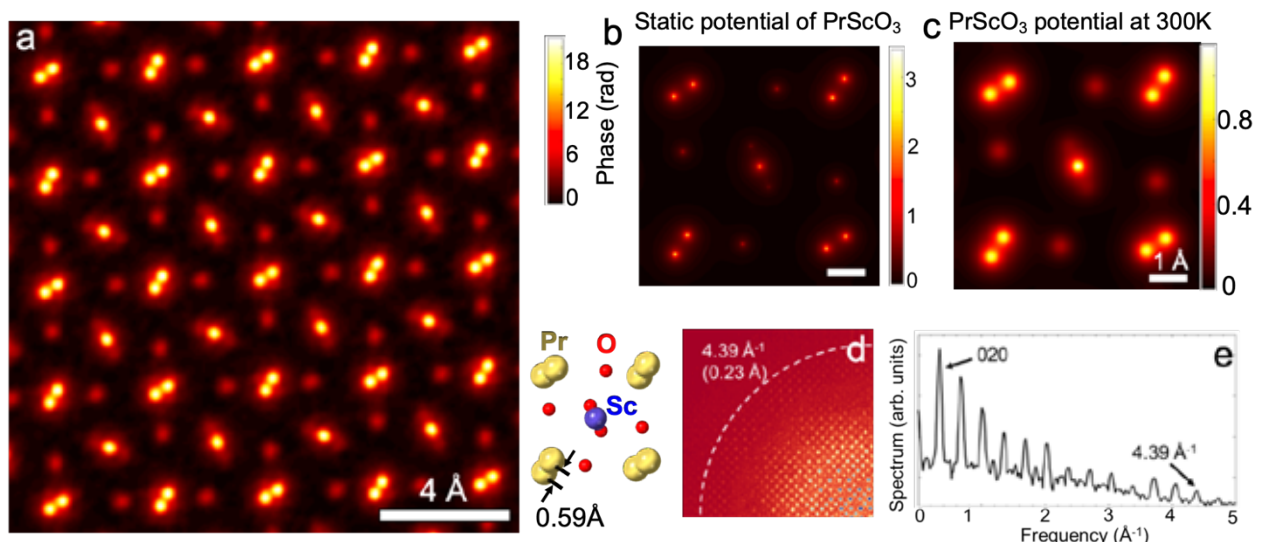


Fig. 1 *Lattice-vibration-limited resolution from multislice ptychography.* (a). Multislice ptychographically-reconstructed phase image from an experimental dataset acquired from a 21 nm thick PrScO_3 sample. (b) static potential neglecting zero-point fluctuations, (c) Projected Potential calculated including thermal vibrations at 300 K. (d) Diffractogram of the phase image from experiment and (e) a line profile cut through d on a log scale.

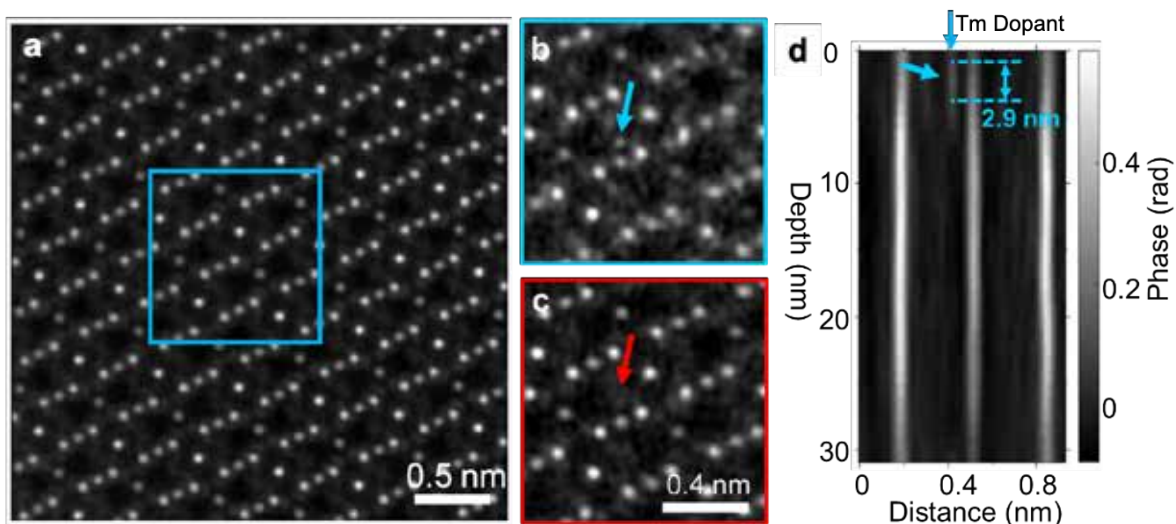


Fig. 2 (a) Multislice ptychographic reconstruction of a $\text{Gd}_3\text{Ga}_5\text{O}_{12}$ film near an interface with $\text{Tm}_3\text{Fe}_5\text{O}_{12}$. Phase image at depths $z=4$ nm (b) and $z=6$ nm (c) within the blue box from (a). The red and blue arrows mark the location of an interstitial Tm atom 2nm apart in depth. (d) Depth variation of phase intensity across one dopant along a cut in the vertical direction. The data was acquired using a probe-forming semi-angle of 21.4 mrad at 300 kV.

References

- [1] P. E. Batson, N. Dellby, and O. L. Krivanek, *Nature* **418**, 617 (2002).
- [2] M. Haider, S. Uhlemann, E. Schwan, H. Rose, B. Kabius, K. Urban, and H. Rose, *Nat.* **392**, 768 (1998).
- [3] Z. Chen, Y. Jiang, Y.-T. Shao, M. E. Holtz, M. Odstrčil, M. Guizar-Sicairos, I. Hanke, S. Ganschow, D. G. Schlom, and D. A. Muller, *Science* **372**, 826 (2021).
- [4] Z. Chen, M. Odstrcil, Y. Jiang, Y. Han, M.-H. Chiu, L.-J. Li, and D. A. Muller, *Nat. Commun.* **11**, 2994 (2020).
- [5] P. M. Pelz, W. X. Qiu, R. Bücke, G. Kassier, and R. J. D. Miller, *Sci. Rep.* **7**, 9883 (2017).
- [6] A. M. Maiden, M. J. Humphry, F. Zhang, and J. M. Rodenburg, *J. Opt. Soc. Am. A* **28**, 604 (2011).
- [7] A. M. Maiden and J. M. Rodenburg, *Ultramicroscopy* **109**, 1256 (2009).
- [8] P. D. Nellist and J. M. Rodenburg, *Ultramicroscopy* **54**, 61 (1994).
- [9] Y. Jiang, Z. Chen, Y. Han, P. Deb, H. Gao, S. Xie, P. Purohit, M. W. Tate, J. Park, S. M. Gruner, V. Elser, and D. A. Muller, *Nature* **559**, 343 (2018).
- [10] S. Gao, P. Wang, F. Zhang, G. T. Martinez, P. D. Nellist, X. Pan, and A. I. Kirkland, *Nat. Commun.* **8**, 1 (2017).
- [11] M. Schloz, T. C. Pekin, Z. Chen, W. Van den Broek, D. A. Muller, and C. T. Koch, *Opt. Express* **28**, 28306 (2020).
- [12] J. J. Donatelli and J. C. H. Spence, *Phys. Rev. Lett.* **125**, 065502 (2020).

Research supported by US NSF (grants DMR-1539918 and DMR-1719875).

Session F:

Electron Beam Shaping

Electron Energy Loss Spectroscopy with an Orbital Angular Momentum sorter: results and challenges

E. Rotunno¹

¹ *S3, Istituto di nanoscienze-CNR, Modena, Italy*

Introduction

Historically, the evolution of the electron optics in microscopy has been characterized by major leaps forward. Such important steps include the invention of spherical aberration correction systems [1], the development of the chromatic aberration corrector [2] and the introduction of monochromators [3].

One of the most significant recent developments is electron beam shaping through electron optical components based on microelectromechanical systems technology [4].

These electronic devices are installed directly inside the microscope's columns and have been used to generate vortex beams [5], non-diffracting beams [6], compact aberration correctors [7] and quantum state analysers [8].

The most prominent application of such techniques is probably the orbital angular momentum (OAM) sorter [9], which makes use of electron beam shaping to measure an electron beam's component of OAM in the propagation direction by decoupling the azimuthal and radial degrees of freedom.

The introduction of the OAM sorter has been predicted to positively impact on many electron microscopy fields: from imaging [10] to more exotic experiments [11]. However is on the field of Electron Energy Loss Spectroscopy (EELS) that the sorter has its main impact.

It is in fact, desirable to add a second dispersion variable to produce a momentum and energy double dispersion EELS or acquire a spectrum for a given momentum transfer [12].

The OAM along the main electron propagation direction is a natural choice being rotational symmetry the natural symmetry of atoms.

The possibility to perform double dispersed OAM-Energy experiments makes new measurements feasible. Among these we can mention the study of Electron Magnetic Circular Dichroism (EMCD) [13], the excitation of Plasmon with specific OAM and plasmonic dichroism. [14]

Methods

The experimental setup needed to simultaneously disperse the inelastically scattered electrons along two orthogonal directions, according to their energy and orbital momentum respectively is described in fig.1.

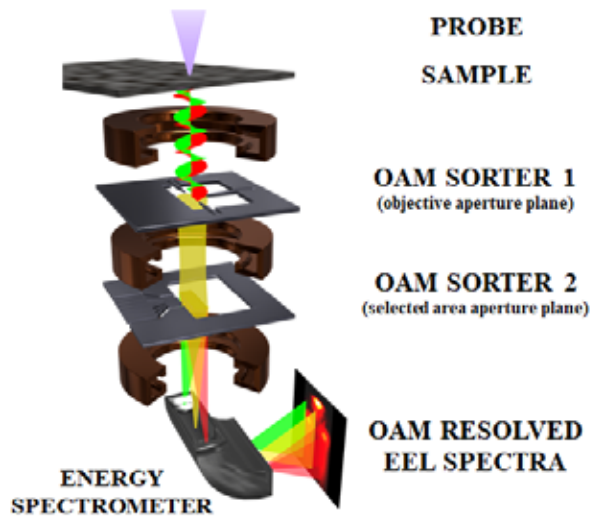


Fig. 1: Scheme of the experimental apparatus: the sample is located in the standard sample position, the first sorter element is located in the objective aperture plane and the second element in the SAD aperture. The sorter is oriented in such a way that the OAM dispersion direction is orthogonal to the energy dispersion direction.

Results

Figure 2 shows the advantage of the OAM sorter in the application to 2D anisotropic materials (B-K edge of a [001] oriented hexagonal Boron Nitride).

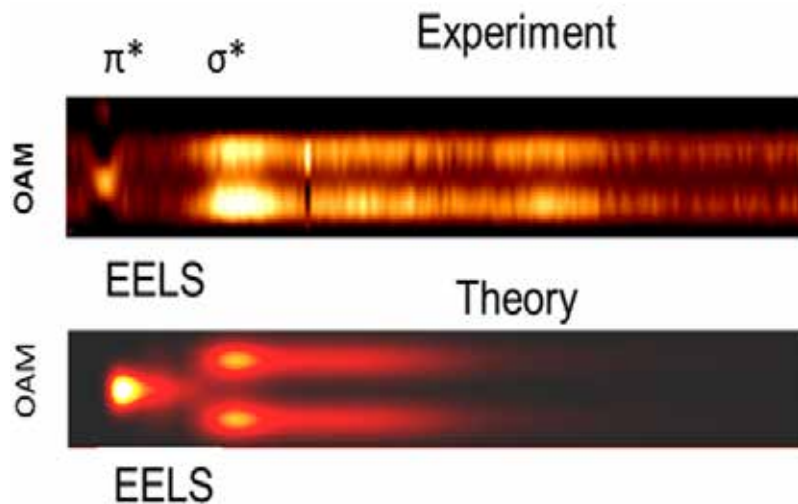


Fig.2 Comparison between experimental and theoretical B-K edge OAM-EEL spectrum of a [001] oriented hexagonal Boron Nitride

According to preliminary simulations based on the symmetry of the partial density of states (pDOS) as implemented in the standard DFT methods, the combined OAM-EELS spectra show a distinct difference between transition $1s \rightarrow \sigma$ ($l = -1, +1$) and $1s \rightarrow \pi$ ($l = 0$) transitions. In this case the advantage of the sorter is to allow for a direct separation of the two contributions in a single acquisition, while normally this would require a tilt of the

specimen in the standard (q, E) basis to separate the two overlapping features, which may be not possible in the experimental setup.

Conclusion

Combining the ability of the OAM sorter to measure an electron beam's component of OAM in the propagation direction together with conventional energy loss spectroscopy, provides a new powerful tool for materials' investigation.

Application such as of Electron Magnetic Circular Dichroism (EMCD), the excitation of Plasmon with specific OAM and plasmonic dichroism will be discussed.

References

- [1] M. Haider, et al. *Nature* **392**, 768 (1998)
- [2] M. Haider, et al. *Ultramicroscopy* **108**, 167-178 (2008)
- [3] P.C. Tiemeijer, et al. *Ultramicroscopy* **114**, 72-81 (2012)
- [4] J. Verbeeck et al. *Ultramicroscopy*, **190**, 58–65 (2018)
- [5] A. H. Tavabi, et al. *Phys. Rev. Research* **2**, 013185 (2020)
- [6] V. Grillo, et al. *Phys. Rev. X* **4**, 011013 (2014)
- [7] V. Grillo et al. *Opt. Express* **25**, 21851 (2017)
- [8] A.H. Tavabi et al. *Phys. Rev. Lett.* **126**, 094802 (2021)
- [9] B.J. McMorrان, *New J. Phys.* **19**, 023053 (2017).
- [10] F. Troiani et al. *Phys. Rev. A* **102**, 043510 (2020)
- [11] E. Rotunno *et al.* *Microsc. Microanal.* **26**, 236-238 (2020)
- [12] Senga, R.,et al. *Nature* **573**, 247–250 (2019)
- [13] Rotunno et al. *Physical Review B* **100**, 224409 (2019)
- [14] M. Zanfagnini *et al.* *ACS Photonics* **6**, 620-627 (2019)

Optical polarization analogue in free electrons beams

H. Lourenço-Martins^{1,2}, D. Gérard³ and M. Kociak¹

¹*Laboratoire de Physique des Solides, Université Paris-Sud, CNRS-UMR 8502, Orsay 91405, France*

²*University of Göttingen, IV. Physical Institute, Göttingen, Germany*

³*Light, nanomaterials, nanotechnologies (L2n), CNRS-ERL 7004, Université de Technologie de Troyes, Troyes 10000, France*

Classical wave optics and quantum mechanics share strong similarities rooted in the underlying - Helmholtz or Schrödinger - wave equations [1]. This very close resemblance is e.g. directly translated in the great amount of optical-electronic analogue phenomena, from the much celebrated Young-Feynman double-slits experiment [2, 3] to more exotic yet fascinating examples such as corrals [4, 5], whispering-gallery-modes [6, 7], quantum spin Hall effect [8, 9] or Anderson localization [10, 11] to name a few. This mesmerizing analogy initiated a long standing and fruitful dialogue between these two fields. A famous example is the development of transmission electron microscopy (TEM), strongly inspired by optical concepts [12]. Conversely, electron microscopy also influenced its photonic counterpart through the discovery of holography [13]. This mutual influence culminated a decade ago when electron vortices have been predicted [14] and measured [15, 16] - these exotic beams constituting a canonical example of a generic wave phenomenon first observed with light [17].

This analogy was more recently extended to the inelastic interaction of light or electrons with matter. Indeed, the Electron energy loss spectroscopy (EELS) has long been used to measure plasmons absorption [18]. However, in the case of photonic excitations such as plasmons, it is only with recent technological advances that a full mapping of the broad band optical properties at very deep sub-wavelength scale has been made possible in the NIR-UV regime [19, 20] then extended to the far-IR domain [21]. Beyond these key experimental advantages over photon based optical spectroscopies, the success of EELS relies heavily on the very solid theoretical foundations that permit to directly interpret experimental results in terms of well-known macroscopic and nanoscopic optical quantities. Indeed, EELS has been shown to be directly related to the extinction cross section on the one hand, and intimately connected to the nanoscale concept of total electromagnetic local density of states - EMLDOS- [22]. Nevertheless, EELS in an electron microscope is seriously hindered by its well-known inability to measure the polarization of photonic excitations, which is rooted in the scalar character of the Schrödinger

equation. Now, the importance of polarization effects at the nanoscale is not to be demonstrated. For example, the measurement of circular dichroism, permits to identify different molecules enantiomers, an information of paramount importance two different enantiomers can be either a cure or a poison. Plasmonic nanostructure can increase circular dichroism beyond that of a pure circular wave plane on scale much smaller than a typical light wavelength therefore giving hope for much better molecular sensors [23]. Developing a polarized EELS (pEELS) could potentially shine light on sometimes controversial [24] nanoscale polarization effects such as the super-chirality [23], i.e the local enhancement of circular dichroism beyond what is possible with a circularly polarized plane wave.

In a visionary work, Asenjo-Garcia and Garcia de Abajo [25] demonstrated that a circular dichroic signal can be measured on chiral assemblies of metallic nanoparticles, much like it was demonstrated with photons in the seminal work on dichroic assembly of metallic nanoparticles [26]. Later, the use of π beams, i. e. singular electron beams with a π -like symmetry in the plane perpendicular to the electron propagation direction was used to mimick a optical polarization depend experiment in EELS [27]. Both works were relating on theories were the interaction was described as the transition of the incoming phase shaped wave to a plane wave. This selection-rule based approach is similar in essence, although based on different physical assumptions [28], to that developed for describing dichroic signal in the so-called core-loss EELS [29]. All together, these pioneering works, as well as the phenomenological work of Ugarte et Ducati [30] and the numerical investigation of Zanfrognini and collaborators [31] gave important hints on the relation between the symmetry of free electron beams and optical polarization. Unfortunately, they did not relate the EELS probabilities to any universal macroscopic or nanoscopic photonic observable. Additionally, it remained unclear what physical vectorial quantity for free electrons shall be used as an analogue to optical polarisation.

In this talk, we will essentially describe the theoretical results presented in [32]. We will show that we can rigorously define an optical polarization analogue (OPA) for fast electrons as a vector equal to the transition dipole between two phase-shaped states. We will then investigate the case where the beam waist of the electron beam w_0 is larger or comparable to the typical variation length of the probed nano-optical field L . In this case, we can demonstrate that the polarized EELS and the linear/circular optical extinction cross-sections can be directly connected, provided that incoming and outgoing electron states are properly defined.

Particularly, we will show the perfect analogy of the role of linear polarization dephasing upon wave propagation in the observation of circular dichroism in pEELS and LES (see Fig. 1). In the case of nanoscale electron beams ($w_0 \ll L$) we will show that pEELS measures the EMLDOS polarized linearly or circularly in the direction perpendicular to the electron

propagation axis. This result sharply contrasts with conventional EELS experiments, which only access the component of the EMLDOS oriented along the beam propagation axis. Additionally, we will demonstrate that the circular dichroism in pEELS is proportional to the local density of spin of the nano-optical field.

Eventually, if time permits, we will discuss experimental geometries that will be needed to explore pEELS.

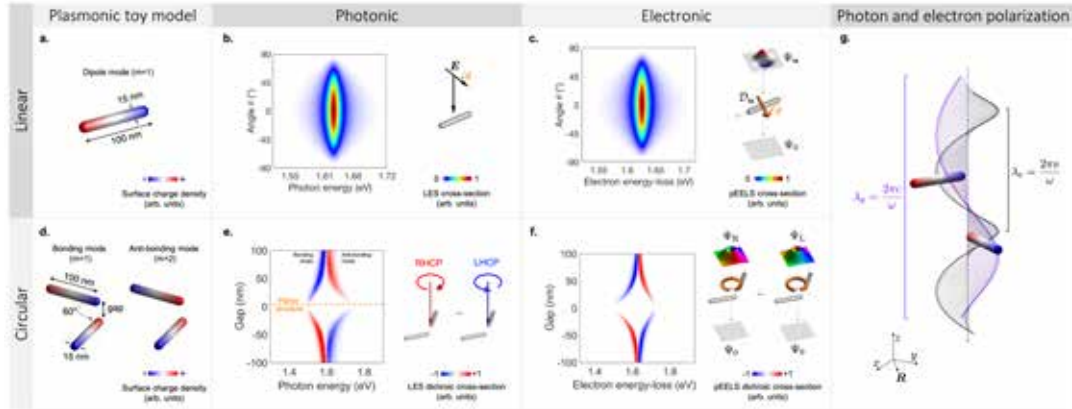


Figure 1: Comparison of linear (top) and circular (bottom) polarized light extinction spectroscopy (LES) and non-spatially resolved pEELS experiments on simple plasmonic nano-structures - **a.** Silver antenna sustaining a dipolar plasmon mode. Malus law measured on the antenna with **b.** light (LES) and **c.** electronic (pEELS) excitations. In this case, the electron beam is centered in the middle of the antenna. **d.** The simplest three-dimensional optically active plasmonic structure is built by combining two antennas similar to the one of **a.** These two antennas form an angle 60° and are offset along z by a variable distance denoted as the gap. The activity increases with decreasing gap, in the same manner for **e.** optical and **f.** electronic measurements. In this case, the electron beam is centered on the tips of the two antennas. **g.** Schematics showing the propagation of a planewave of wavelength λ_p (purple line) and of an effective electron transition current of wavelength λ_e (black line) along a BKS nano-structure.

References

- [1] E. Akkermans, G. Montanboux, *Physique mésoscopique des électrons et des photons*, Savoirs actuels (EDP Sciences, 2012).
- [2] A. Tonomura, J. Endo, T. Matsuda, T. Kawasaki, H. Ezawa, *American Journal of Physics* **57**, 117 (1989).
- [3] R. Bach, D. Pope, S.-H. Liou, H. Batelaan, *New Journal of Physics* **15**, 033018 (2013).
- [4] M. F. Crommie, C. P. Lutz, D. M. Eigler, *Science* **262**, 218 (1993).
- [5] G. Colas des Francs, *et al.*, *Physical Review Letters* **86**, 4950 (2001).
- [6] K. J. Vahala, *Nature* pp. 839–846 (2003).

- [7] G. Reecht, *et al.*, *Physical Review Letters* **110**, 1 (2013).
- [8] X. Qian, J. Liu, L. Fu, J. Li, *Science* **346**, 1344 (2014).
- [9] K. Y. Bliokh, D. Smirnova, F. Nori, *Science* **348**, 1448 (2015).
- [10] P. W. Anderson, *Physical Review* **109**, 1492 (1958).
- [11] D. S. Wiersma, P. Bartolini, A. Lagendijk, R. Righini, *Nature* **390**, 671 (1997).
- [12] M. Haider, *et al.*, *Nature* **392**, 768 (1998).
- [13] D. Gabor, *Nature* **161**, 777 (1948).
- [14] K. Y. Bliokh, Y. P. Bliokh, S. Savel'ev, F. Nori, *Phys. Rev. Lett.* **99**, 190404 (2007).
- [15] J. Verbeeck, H. Tian, P. Schattschneider, *Nature* **467**, 301 (2010).
- [16] B. J. McMorran, *et al.*, *Science* **331**, 192 (2011).
- [17] L. Allen, M. W. Beijersbergen, R. J. C. Spreeuw, J. P. Woerdman, *Phys. Rev. A* **45**, 8185 (1992).
- [18] P. E. Batson, *Phys. Rev. Lett.* **49**, 936 (1982).
- [19] J. Nelayah, *et al.*, *Nature Physics* **3**, 348 (2007).
- [20] M. Bosman, V. J. Keast, M. Watanabe, A. I. Maaroof, M. B. Cortie, *Nanotechnology* **18**, 165505 (2007).
- [21] D. Rossouw, G. A. Botton, *Physical Review Letters* **110**, 66801 (2013).
- [22] F. J. García de Abajo, M. Kociak, *Physical Review Letters* **100**, 106804 (2008).
- [23] R. Tullius, *et al.*, *Journal of the American Chemical Society* **137**, 8380 (2015).
- [24] S. M. Kim, G. Gbur, *Physical Review A - Atomic, Molecular, and Optical Physics* **86**, 1 (2012).
- [25] A. Asenjo-Garcia, F. J. García De Abajo, *Physical Review Letters* **113**, 1 (2014).
- [26] X. Shen, *et al.*, *Nano Letters* **13**, 2128 (2013).
- [27] G. Guzzinati, *et al.*, *Nature Communications* **8**, 14999 (2017).
- [28] H. Lourenço-Martins, A. Lubk, M. Kociak, *SciPost Physics* **10**, 1 (2021).
- [29] P. Schattschneider, S. Löffler, M. Stöger-Pollach, J. Verbeeck, *Ultramicroscopy* **136**, 81 (2014).
- [30] D. Ugarte, C. Ducati, *Physical Review B* **93**, 1 (2016).
- [31] M. Zanfrognini, *et al.*, *ACS Photonics* **6**, 620 (2019).
- [32] H. Lourenço-Martins, D. Gérard, M. Kociak, *Nature Physics* **17**, 598 (2021).

Electron beam aberration correction and shaping using optical fields

A. Konečná¹ and F. J. García de Abajo^{1,2}

¹ICFO-Institut de Ciències Fotoniques, The Barcelona Institute of Science and Technology, 08860 Castelldefels (Barcelona), Spain

²ICREA-Institució Catalana de Recerca i Estudis Avançats, Passeig Lluís Companys 23, 08010 Barcelona, Spain

Introduction

Over last decades, electron microscopy has become very powerful and versatile technique for nano- or atomic-scale imaging and spectroscopy [1]. Major advancements and outstanding capabilities have been made possible thanks better spatial and temporal control over the amplitude and phase of the wave function that characterizes the fast electrons used as sample probes. Control over the beam shape is commonly achieved by means of complex arrangements of magneto- and electrostatic electron lenses that enable sub-Ångstrom focusing and beam scanning, as well as correcting aberrations of electron optics. The phase of the electron wave function can be additionally modified by introducing static phase plates.

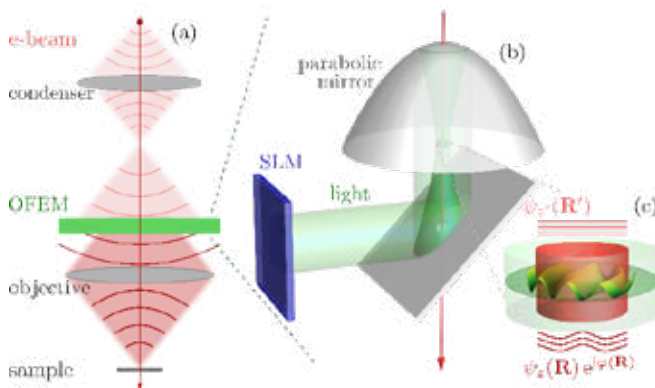


Fig. 1 Optical free-space electron modulator (OFEM). (a) The proposed element is placed in the electron microscope column right before the objective lens. (b) The OFEM incorporates a parabolic mirror that focuses light with a high numerical aperture on a vacuum region that intersects the electron beam. The electric field distribution at the optical focal spot is patterned by using a far field spatial light modulator (SLM). (c) A phase is imprinted on the electron wave function.

Results and Discussion

We envision an alternative to traditional electron-optics elements, materialized in the concept of the optically-driven electron modulator that enables dynamical shaping of electron-beam

wave functions both in space and time. This approach capitalizes recent experimental demonstrations of wave function control through optical fields [2] combined with ultrafast control over the electron-light interaction [3-5]. Specifically, we propose two types of schemes to realize optical control over the electron beam shape: a photonic aberration corrector (PAC) that exploits the interaction of the electron with light scattered from a thin film; and an optical free-space electron modulator (OFEM; see Fig. 1) operating in free space. Based on realistic designs combined with detailed simulations, we demonstrate an application with high potential for improving the resolution of electron microscopes, whereby the electron-light interaction is used to correct for common aberrations introduced by electro- or magneto-static lenses in current setups [6]. In addition, we demonstrate the possibility of generating exotic electron beam shapes [6,7], with the extra advantage that fast control over such shapes is inherent to the optical elements used in our designs.

Our theoretical work suggests that the proposed PAC and OFEM elements could offer better versatility and compactness with respect to traditional static electron phase plates and corrector designs, and we foresee that they could open a new era of electron microscopy, both in aberration correction and in the generation of on-demand electron beams.

References

- [1] P. E. Batson, N. Dellby, and O. L. Krivanek, *Nature* **418**, 617 (2002).
- [2] O. Schwartz, et al., *Nat. Methods* **16**, 1016 (2019).
- [3] B. Barwick, D. J. Flannigan, and A. H. Zewail, *Nature* **462**, 902 (2009).
- [4] A. Feist, K. E. Echternkamp, J. Schauss, S. V. Yalunin, S. Schäfer, and C. Ropers, *Nature* **521**, 200 (2015).
- [5] G. M. Vanacore, et al., *Nat. Mater.* **18**, 573 (2019).
- [6] A. Konečná, and F. J. García de Abajo, *Phys. Rev. Lett.* **125**, 030801 (2020).
- [7] F. J. García de Abajo, and A. Konečná, *Phys. Rev. Lett.* **126**, 123901 (2021).

Recent results in 3D wavefront modulation and quantum mechanical detection

T. Latychevskaia^{1,2} and A. Kohli²

¹Paul Scherrer Institute, 5232 Villigen, Switzerland

²Department of Physics, University of Zurich, 8057 Zurich, Switzerland

Introduction

The presentation consists of two parts, presenting the latest results in: (1) wavefront modulation using inverted Gabor holography with amplitude and phase masks [1, 2], and (2) quantum mechanical structure detection in electron microscopy [3].

Methods

Wavefront modulation using inverted Gabor holography

The concept of inverted Gabor holography for creating arbitrary 3D wavefront distributions was proposed in ref. [1] and illustrated in Fig. 1. The original study considered the wavefront modulation using only amplitude masks (modulator) with transmission $M(X,Y) \propto 1 - H(X,Y)$, where $H(X,Y)$ is an in-line hologram $H(X,Y) = |U(X,Y)|^2$ normalized to values 0 ... 1, $U(X,Y)$ is the complex-valued wavefront distribution in the detector plane. Recently, the same method of wavefront modulations was demonstrated with phase masks $M(X,Y) = \exp\{i\text{Arg}[-U(X,Y) + C]\}$ [2], and the results obtained for both types of masks were compared, Fig. 2.

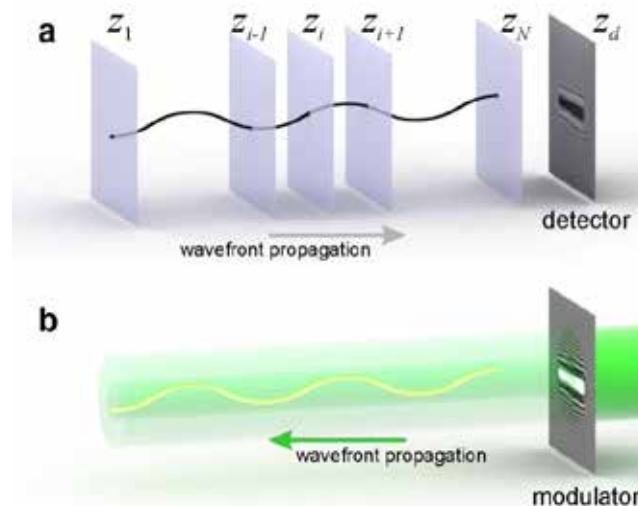


Fig. 1 Three-dimensional (3D) wavefront modulation by inverted Gabor holography principle. (a) A pre-defined 3D curve is sampled in the planes at z_i , $i = 1 \dots N$, providing a distribution of transmission functions $t_i(x, y, z_i)$. Hologram $H(X, Y)$ is simulated by propagating the plane wave through all the planes down

to the detector plane (X, Y) . (b) Reconstruction of the 3D light curve. A plane wave illuminates the modulator, which is a contrast-inverted hologram, and the wavefront behind the modulator is shaped into a 3D intensity distribution.

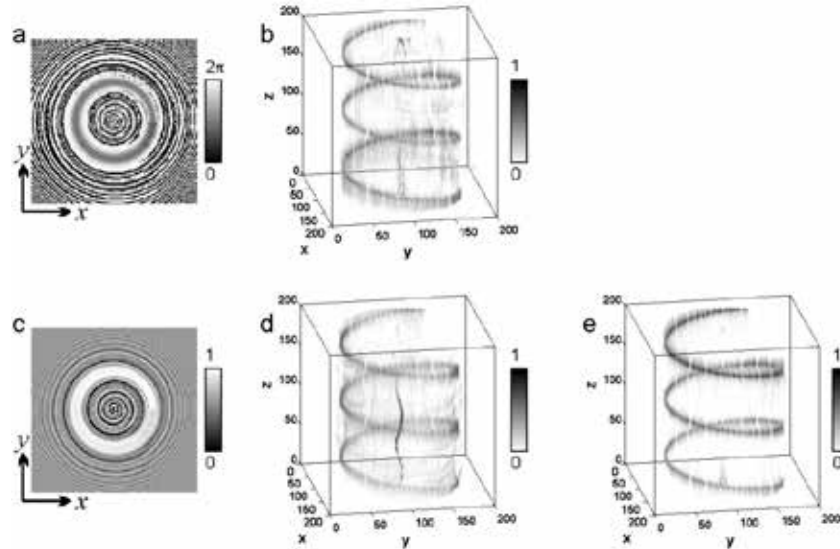


Fig. 2 Three-dimensional (3D) intensity wavefront modulation in the form of a 3D helical structure employing a phase-only modulator, simulated study. (a) Phase distribution loaded on a phase-only modulator. (b) 3D intensity distribution reconstructed behind the modulator. (c) Amplitude distribution loaded on an amplitude-only modulator, and (d) 3D intensity distribution reconstructed behind the modulator. (e) 3D intensity distribution reconstructed behind a complex-valued modulator. For all three modulators: pixel size in the (x, y) plane is $\Delta_{x,y} = 32 \mu\text{m}$, pixel size along the z -axis is $\Delta_z = 4\text{mm}$, total length along the z -axis is 800mm . In (a) and (c) only the central region of 300×300 pixels of 832×832 pixels distribution is shown.

Quantum mechanical imaging in electron microscopy

The concept of verifying macromolecule structure with only a few electrons instead of complete imaging of the structure with a high electron dose was proposed in ref. [3], and illustrated in Fig. 3(a). Our recent numerical simulations demonstrate that under certain geometrical conditions the method is insensitive to the sample lateral shifts: when the sample is shifted, a bright spot is detected on the screen but at a shifted position (Fig. 3(b) - (f)). The bright spot is also detected when the sample is axially shifted or rotated within some range of distances (rotations). A method for structure detection which is insensitive to the sample rotations will be also presented and discussed.

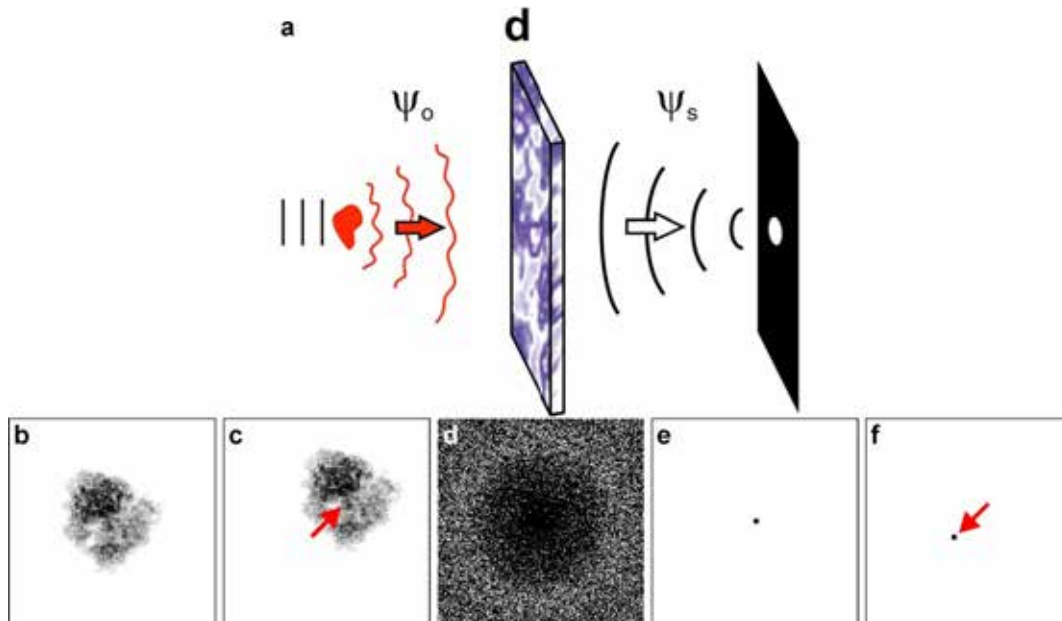


Fig. 3 Quantum mechanical imaging in electron microscopy, simulated study. (a) The principle as explained in ref. [3]. (b) Ribosome structure and (c) laterally shifted structure. (d) Corresponding diffractor (binary mask). (e) and (f) Intensity distributions on the screen when the diffractor is illuminated with the wavefront from the ribosome structure (b) and shifted ribosome structure (c), respectively. Simulations are done for 200 keV electrons, the ribosome structure atomic model is the protein data bank structure 1BRD [4, 5].

References

- [1] T. Latychevskaia, H.-W. Fink, Inverted Gabor holography principle for tailoring arbitrary shaped three-dimensional beams, *Sci. Rep.*, 6 (2016) 26312.
- [2] T. Latychevskaia, Wavefront modulation and beam shaping into arbitrary three-dimensional intensity distributions, *Photonics*, 8 (2021) 179.
- [3] H. Okamoto, T. Latychevskaia, H.-W. Fink, A quantum mechanical scheme to reduce radiation damage in electron microscopy, *Appl. Phys. Lett.*, 88 (2006) 164103.
- [4] R. Henderson, J.M. Baldwin, T.A. Ceska, F. Zemlin, E. Beckmann, K.H. Downing, Model for the structure of bacteriorhodopsin based on high-resolution electron cryo-microscopy, *J. Mol. Biol.*, 213 (1990) 899–929.
- [5] R. Henderson, J.M. Baldwin, T.A. Ceska, F. Zemlin, E. Beckmann, K.H. Downing, PDB ID: 1BRD, (1990) 10.2210/pdb2211BRD/pdb.

Structured Electron Beams for Interaction-free Measurements and Inelastic Interferometry

B. McMorran¹, C. Johnson¹, and A. Turner¹

¹*Department of Physics, University of Oregon, Eugene, Oregon, 97403, USA*

Introduction

Here we report using structured electron beams to probe the coherence and symmetry of inelastic electron scattering as well as demonstrating interaction-free measurements. Structured electron beams are comprised of electrons with engineered phase, amplitude, and momentum. Specialized apertures featuring holographic gratings can be used to structure electron beams in electron microscopes. For example, we use holographic gratings to efficiently prepare electrons with quantized orbital angular momentum (OAM) [1,2], produce electron beams that coil in space [3], remove aberrations [4], or split the electron beam and put electrons in superpositions of separated trajectories [5]. Electron-transparent phase gratings provide a way to efficiently diffract electrons with desired properties in scanning transmission electron microscopes (STEM) [6–8], and amplitude gratings with binary transmission can be used at lower energies in scanning electron microscopes (SEMs) [9].

Imaging individual beam-sensitive materials, such as biomolecules, at atomic resolution with negligible damage has been a long-standing goal in electron microscopy, but it would necessitate a significant dose decrease from current methods as well as improved phase contrast. Exploiting quantum protocols is one possible avenue for achieving damage-free imaging. The Elitzur and Vaidman quantum bomb detector [10] is one proposed mechanism to reduce interactions needed to form an image in electron microscopy [11,12]. Interaction-free measurements involve a single input quantum traversing two paths in an interferometer and self-interfering destructively at an output – blocking or scattering one path disrupts this interference and results in an *increase* in events at the output. We implement this interferometric technique in a TEM using two nanofabricated gratings. We use a similar setup to probe the coherence of plasmonic excitations.

Methods

Nanoscale material phase gratings can serve as beamsplitters for electrons to implement interferometry in a TEM. In one configuration, we use a single grating to implement STEM holography [13,14,5,15] for phase contrast imaging at the nanoscale. The phase grating serves as an amplitude-dividing beamsplitter to prepare a superposition of two STEM probes, one of which transmits through the specimen. The probes are overlapped to form an interference pattern at the imaging detector, from which the relative phase shift between the probes can be extracted. An image of the interference pattern is recorded at each position in a scan of the probes, providing a 4D dataset. In another configuration, a second grating is

used to recombine the separated beams post-specimen, giving rise to discrete outputs in the far-field diffraction pattern to form a Mach-Zehnder interferometer [16].

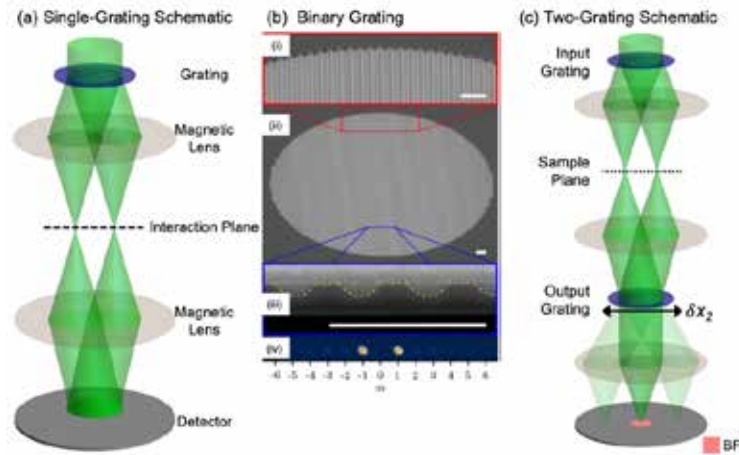


Fig. 1 (a) Schematic of the single-grating configuration for STEM holography. (b) SEM images of the nanofabricated diffraction gratings used in our interferometers, including (iii) a cross-section and the (iv) diffraction efficiency of the grating. (c) Schematic of the two-grating Mach-Zehnder interferometer in a TEM.

Results

Previously, we demonstrated nanoscale phase imaging using STEM holography, identifying nanoscale filamentary features in a carbon substrate, a weak phase object. Recently, we used our two-grating, phase-sensitive interferometer for inelastic interferometry. We utilized the probes to excite the dipole plasmon in a gold nanoparticle and recovered the signal from the elastically and inelastically scattered electrons, respectively. Furthermore, we employed the two-grating interferometer to perform interaction-free measurements with electrons [17,18].

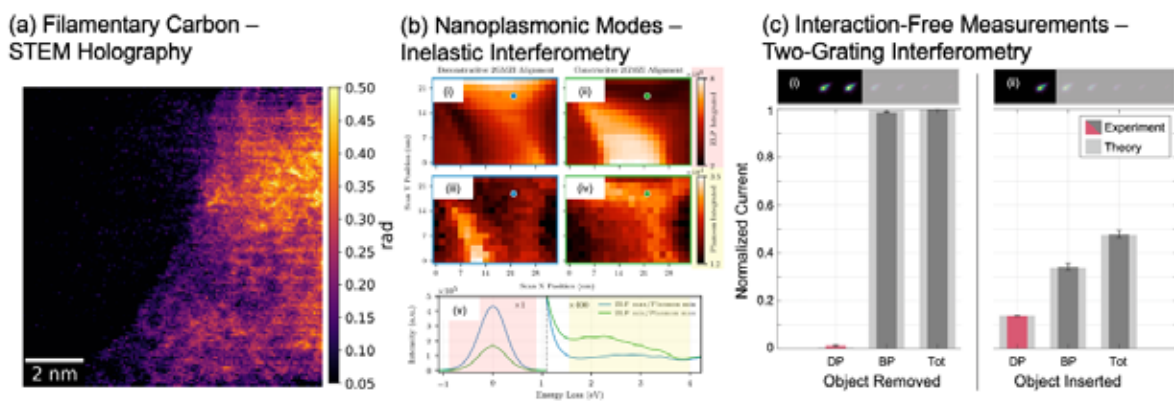


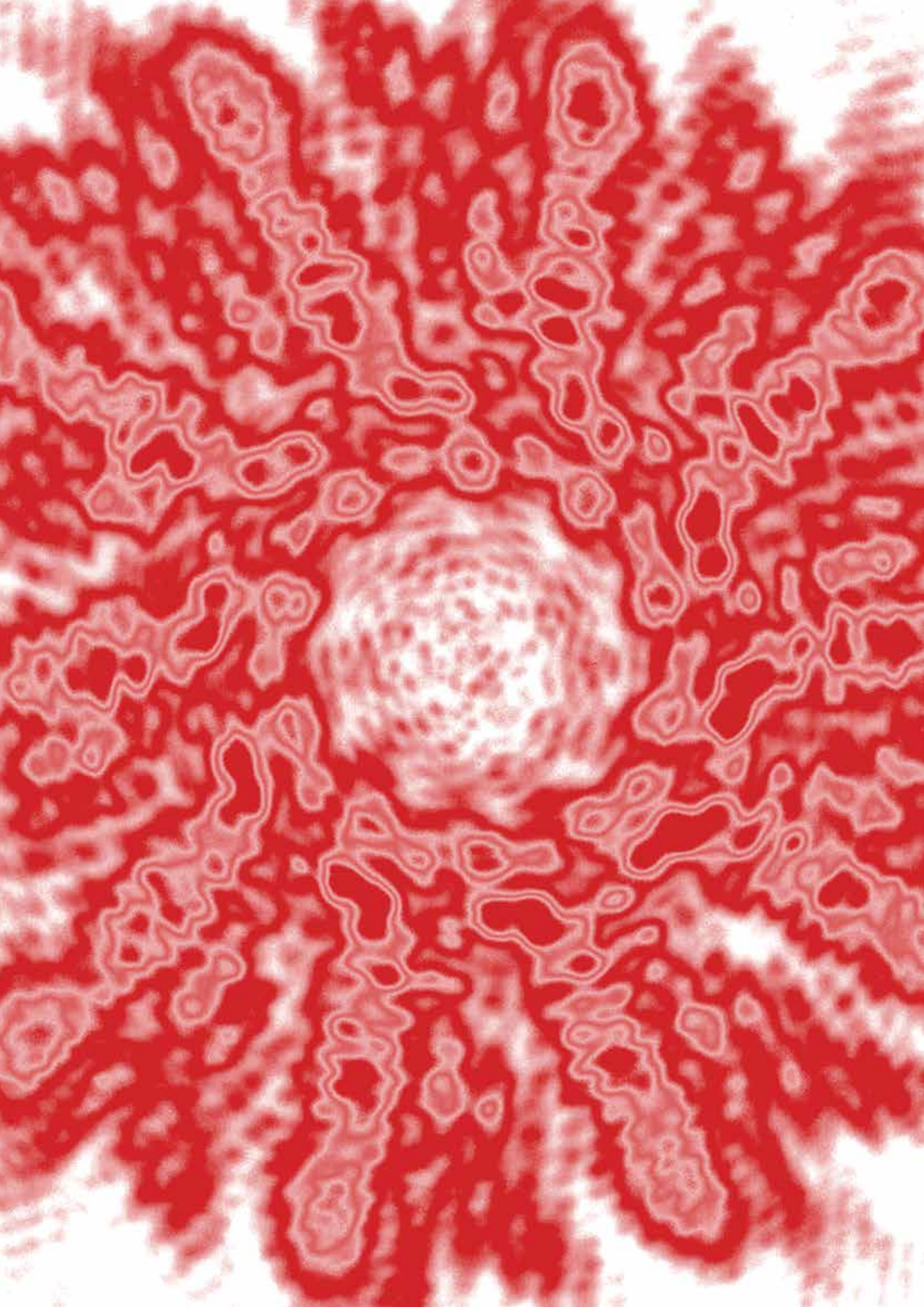
Fig. 2 (a) Filamentary carbon features found using STEM holography (single-grating technique). (b) Spectrum images of a gold nanoparticle for destructive and constructive interferometer alignments, integrating over the zero loss peak and the plasmon peaks. (c) Normalized output currents of the two-grating interferometer with the object removed and inserted, demonstrating interaction-free measurements.

Discussion

These grating-based electron interferometers enable new research prospects, including low-dose high-resolution live interferometric phase imaging, interaction-free electron microscopy [12], probing nanoplasmonic systems, the exploration of decoherence theory [19], interferometric magnetic imaging [20] and Aharonov-Bohm experiments [21].

References

- [1] B. J. McMorran, A. Agrawal, I. M. Anderson, A. A. Herzing, H. J. Lezec, J. J. McClelland, and J. Unguris, *Science* **331**, 192 (2011).
- [2] B. J. McMorran, A. Agrawal, P. A. Ercius, V. Grillo, A. A. Herzing, T. R. Harvey, M. Linck, and J. S. Pierce, *Phil. Trans. R. Soc. A* **375**, 20150434 (2017).
- [3] J. Pierce, J. Webster, H. Larocque, E. Karimi, B. McMorran, and A. Forbes, *New J. Phys.* **21**, 043018 (2019).
- [4] M. Linck, P. A. Ercius, J. S. Pierce, and B. J. McMorran, *Ultramicroscopy* **182**, 36 (2017).
- [5] F. S. Yasin, K. Harada, D. Shindo, H. Shinada, B. J. McMorran, and T. Tanigaki, *Appl. Phys. Lett.* **113**, 233102 (2018).
- [6] T. R. Harvey, J. S. Pierce, A. K. Agrawal, P. Ercius, M. Linck, and B. J. McMorran, *New J. Phys.* **16**, 093039 (2014).
- [7] V. Grillo, G. C. Gazzadi, E. Karimi, E. Mafakheri, R. W. Boyd, and S. Frabboni, *Applied Physics Letters* **104**, 043109 (2014).
- [8] C. W. Johnson, D. H. Bauer, and B. J. McMorran, *Appl. Opt.* **59**, 1594 (2020).
- [9] T. Řiháček, M. Horák, T. Schachinger, F. Mika, M. Matějka, S. Krátký, T. Fořt, T. Radlička, C. W. Johnson, L. Novák, B. Sed'a, B. J. McMorran, and I. Müllerová, *Ultramicroscopy* **225**, 113268 (2021).
- [10] A. C. Elitzur and L. Vaidman, *Found Phys* **23**, 987 (1993).
- [11] W. P. Putnam and M. F. Yanik, *Phys. Rev. A* **80**, 040902 (2009).
- [12] P. Kruit, R. G. Hobbs, C.-S. Kim, Y. Yang, V. R. Manfrinato, J. Hammer, S. Thomas, P. Weber, B. Klopfer, C. Kohstall, T. Juffmann, M. A. Kasevich, P. Hommelhoff, and K. K. Berggren, *Ultramicroscopy* **164**, 31 (2016).
- [13] T. R. Harvey, F. S. Yasin, J. J. Chess, J. S. Pierce, R. M. S. dos Reis, V. B. Özdöl, P. Ercius, J. Ciston, W. Feng, N. A. Kotov, B. J. McMorran, and C. Ophus, *Phys. Rev. Applied* **10**, 061001 (2018).
- [14] F. S. Yasin, T. R. Harvey, J. J. Chess, J. S. Pierce, and B. J. McMorran, *J. Phys. D: Appl. Phys.* **51**, 205104 (2018).
- [15] F. S. Yasin, T. R. Harvey, J. J. Chess, J. S. Pierce, C. Ophus, P. Ercius, and B. J. McMorran, *Nano Lett.* **18**, 7118 (2018).
- [16] C. W. Johnson, A. E. Turner, and B. J. McMorran, *ArXiv:2104.09992 [Physics, Physics:Quant-Ph]* (2021).
- [17] A. Turner, C. Johnson, and B. McMorran, *Microscopy and Microanalysis* **26**, 1744 (2020).
- [18] A. E. Turner, C. W. Johnson, P. Kruit, and B. J. McMorran, *Physical Review Letters* (**accepted**), (2021).
- [19] P. Schattschneider and S. Löffler, *Ultramicroscopy* **190**, 39 (2018).
- [20] A. T. Greenberg, *The Application of Interferometric Electron Microscopy for Nanomagnetic Imaging*, Ph. D. dissertation, University of Oregon, 2020.
- [21] A. Tonomura, N. Osakabe, T. Matsuda, T. Kawasaki, J. Endo, S. Yano, and H. Yamada, *Phys. Rev. Lett.* **56**, 792 (1986).



Session G:

Electron-radiation
interaction

Engineering the wavefunction of electrons for new microscopy methods

F. Carbone

¹ Laboratory for Ultrafast Microscopy and Electron Scattering (LUMES), EPFL, Switzerland

Introduction

In this seminar, we will review some recent results obtained by combining laser pulses with ultrashort electron bunches.

The manipulation of the wavefunction of individual electrons by light allows for the generation of ultrashort electron pulses, as well as the creation of beams carrying orbital angular momentum.

These advanced beams have a variety of applications ranging from magnetic imaging, electron spectroscopy and even nuclear spectroscopy.

Few examples of recent results obtained in these domains will be discussed.

Homodyne detection of cathodoluminescence

O. Kfir¹

¹*School of Electrical Engineering, Tel Aviv University, Tel Aviv, Israel*

Introduction

Cathodoluminescence (CL) offers intriguing coherence properties. Originating from a spontaneous process in a deep subwavelength region, it is generally temporally incoherent, albeit with exquisite spatial coherence. Thus, CL can be interfered with itself spatially and spectrally [1–3], but not with an external laser field. Coherent mixing with a strong local-oscillator at a controllable phase delay would offer an opportunity to fully reconstruct the photonic Wigner distribution or density matrix of CL, for example by optical homodyne tomography [4].

This work proposes a route towards homodyne detection and quantum-state tomography schemes using temporally coherent cathodoluminescence, emitted by electrons that underwent optical coherent modulation through PINEM (photon-induced nearfield electron microscopy) [5,6]. My talk will address the mutual coherence properties of CL concerning the PINEM-driving laser, and its derivation from the multi-energy quantum electron state. Phase-coherent CL arises from the attosecond-structuring of the electron density modulation [7], regardless of the exact timing of the electron wavepacket centroid (see Figure 1a).

The suggested approach comprises an unbalanced homodyne detection of the coherent CL emission using a replica of the PINEM driver, or its harmonics, detected by the difference signal in a pair of photodiodes (see Figure 1b). The electron beam can be considered as substituting an optical path in a Mach-Zehnder interferometer [8,9]. As a fundamentally different physical entity introduced to optical interferometers, the electron adds nontrivial properties such as an inherent nonlinearity, and an oscillatory coupling amplitude with the coherent CL emission. Homodyning allows the amplification of the typically weak CL signal while suppressing the shot noise from the local oscillator [10], and can be extended to a full reconstruction of the CL quantum state. I elaborate on the advantages of collecting nonresonant CL in waveguides [11,12], as they can be easily integrated with complex optical setup, with high fidelity and photon collection efficiently.

I believe that quantum state tomography based on homodyne detection of CL would provide insights into the state of the electron that stimulated the radiation. As non-destructive projective quantum measurements, homodyne mixing schemes can post-select a particular electronic quantum state, for the analysis of its interaction with an individual nanoscale quantum entity.

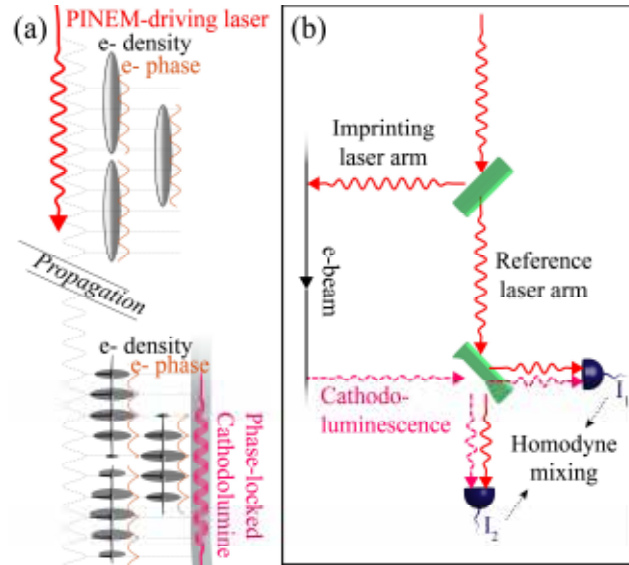


Figure 1 – The mutual coherent between a laser beam and CL. (a, top) The PINEM-driving laser structures the electron phase, which forms (bottom) propagation-dependent density modulations. The CL has partial coherence with respect to the electron density, and hence, with respect to the laser. (b) The mutually coherent part of CL from a modulated electron can be analyzed by homodyne mixing. The suppression of excess shot-noise in this scheme, alongside the scanning of the phase between the laser and the CL allows to reconstruct the CL state at the limit of its quantum uncertainty.

References

- [1] N. Talebi, S. Meuret, S. Guo, M. Hentschel, A. Polman, H. Giessen, and P. A. van Aken, *Nat. Commun.* **10**, 1 (2019).
- [2] T. Sannomiya, A. Konečná, T. Matsukata, Z. Thollár, T. Okamoto, F. J. García de Abajo, and N. Yamamoto, *Nano Lett.* **20**, 592 (2020).
- [3] N. J. Schilder, H. Agrawal, E. C. Garnett, and A. Polman, *ACS Photonics* **7**, 1476 (2020).
- [4] D. T. Smithey, M. Beck, M. G. Raymer, and A. Faridani, *Phys. Rev. Lett.* **70**, 1244 (1993).
- [5] B. Barwick, D. J. Flannigan, and A. H. Zewail, *Nature* **462**, 902 (2009).
- [6] A. Feist, K. E. Echternkamp, J. Schauss, S. V. Yalunin, S. Schäfer, and C. Ropers, *Nature* **521**, 200 (2015).
- [7] K. E. Priebe, C. Rathje, S. V. Yalunin, T. Hohage, A. Feist, S. Schäfer, and C. Ropers, *Nat. Photonics* **11**, 793 (2017).
- [8] O. Kfir, V. D. Giulio, F. J. G. de Abajo, and C. Ropers, *Sci. Adv.* **7**, eabf6380 (2021).
- [9] V. Di Giulio, O. Kfir, C. Ropers, and F. J. García de Abajo, *ACS Nano* **15**, 7290 (2021).
- [10] H. P. Yuen and V. W. S. Chan, *Opt. Lett.* **8**, 177 (1983).
- [11] X. Bendaña, A. Polman, and F. J. García de Abajo, *Nano Lett.* **11**, 5099 (2011).
- [12] O. Kfir, *Phys. Rev. Lett.* **123**, 103602 (2019).

Complex phase space manipulation of pulsed electron beams in a nanophotonic structure

R. Shiloh, T. Chlouba, J. Illmer, N. Schönenberger, P. Yousefi, A. Tafel, J. Litzel, S. Kraus, L. Brückner, B. Löhrl, P. Hommelhoff

Friedrich-Alexander-Universität Erlangen-Nürnberg, Erlangen, Germany, EU

Nanophotonic structures driven with ultrashort laser pulses are ideally suited to control free electrons on ultrafast time scales. We will give an overview on our quest to build a particle accelerator on a chip. Next to acceleration elements, this entails beam steering and beam confinement, all with optical nearfield forces. We will demonstrate attosecond pulse train generation as well as alternating phase focusing, representing complex electron phase space control mandatory for any particle accelerator. Alternating phase focusing is a scheme to confine an electron pulse in all dimensions, and is a prerequisite not to lose electrons while they are accelerated. With the demonstration of this scheme, the particle accelerator on a chip seems within reach. We will show the current status of the experiment.

If times permits, we will show free space control of an electron beam based on two-photon—electron interactions, rendering the otherwise required nearfield structures obsolete. Next to large achievable gradients, we will also show attosecond pulse train generation.

Tunable Photo-Induced Free-Electron Spatial Modulation

**Shai Tsesses¹, Raphael Dahan¹, Kangpeng Wang¹, Ori Reinhardt¹,
Guy Bartal¹ and Ido Kaminer¹**

¹*Technion – Israel Institute of Technology, Haifa, Israel*

Spatially shaping electron beams has great importance in industrial and academic applications, such as nanolithography, microscopy, material studies and fabrication inspection. To this end, the frontier of research in recent years has been spatial coherent shaping, achieved via phase and amplitude holograms for electrons [1-3]. Recently, a new method to generate such spatial electron modulation was proposed, based on the ultrafast interaction of electron pulses and near-field electromagnetic waves [4,5], attracting attention for the ability to correct and purify electron beams [6,7]. Tunable spatial modulation of electron beams, on the other hand, is still an open challenge by any means [8] and has yet to be performed experimentally with electron-light interactions.

Here, we present active spatial modulation of electrons by engineering their interaction with ultrafast surface plasmon interference patterns in an ultrafast transmission electron microscope (UTEM). First, in the linear interaction regime, we directly determine the electron distribution through shaping of the plasmonic field, by engineering the plasmonic coupling slit or the polarization of the laser pulse impinging it. Thereafter, in the nonlinear interaction regime [9], we demonstrate how different interaction orders possess a different shape, while the entire electron distribution undergoes 2D spatial Rabi oscillations [10,11]. Our work presents new degrees of freedom to actively shape electron wavefunctions, with possibilities for improving state-of-the-art electron microscopy with tunable and tailored electron beams.

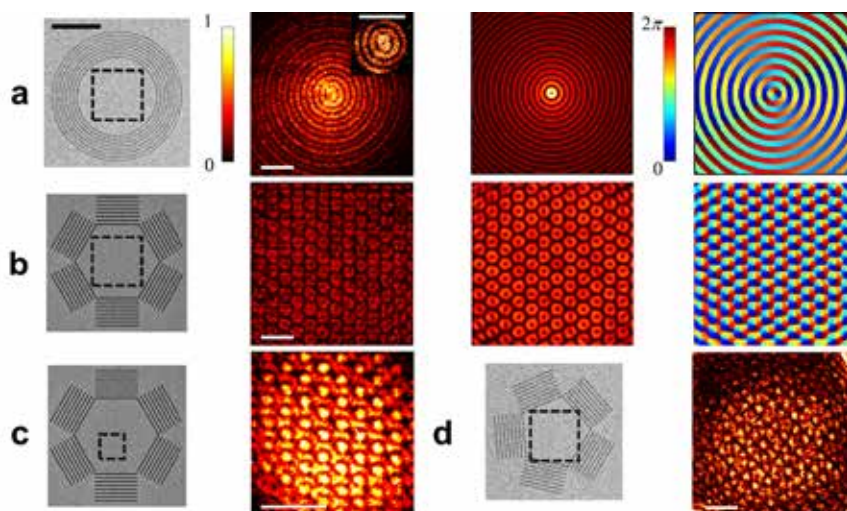


Fig. 1. Passive spatial modulation free electrons. The figure shows the spatial probability distribution of ~ 300 fs electron wavepackets after interaction with the near field of various plasmonic patterns. The near field is excited via 20 mW, ~ 250 fs laser pulses in nearly-circular

polarization and with a central wavelength of 730 nm. Different coupling slit geometries lead to different distributions: (a) a 1st-order Bessel electron vortex, (b) a hexagonal electron vortex array, (c) a hexagonal electron foci array and (d) a quasi-periodic pentagonal distribution. Each electron distribution is coupled with an SEM micrograph of the coupling slit used to generate it. The measurement area is marked in every micrograph by a dashed square. Inset (a) is an image of the measured distribution, taken at a larger magnification, where the vortex singularity is more clearly visible. The measurements in (a),(b) are also complemented by their corresponding calculated probability distribution and phase. The black scale bar (relevant to all SEM micrographs) corresponds to 10 microns. All white scale bars correspond to 2 microns. Energy filtering window is 10 eV wide, on the gain side (centered around -8 eV).

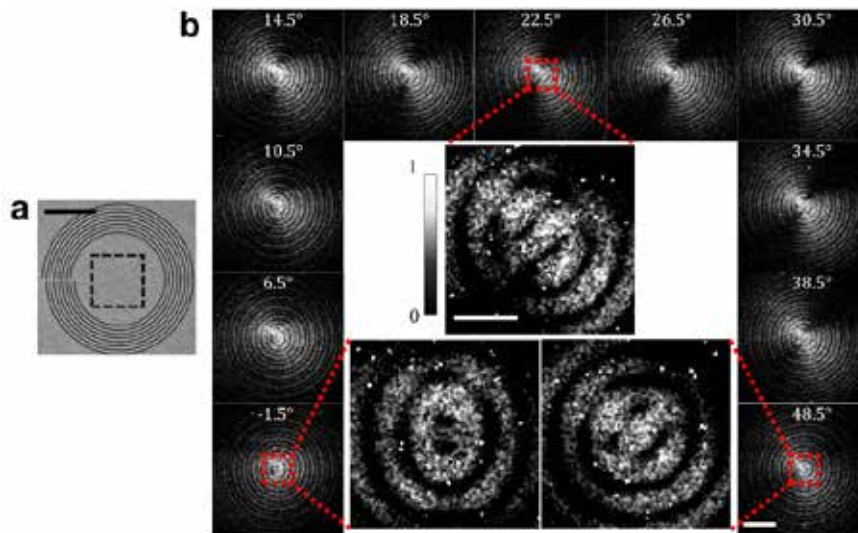


Fig. 2. Active spatial modulation of electron wavepackets using polarization control. (a) An SEM micrograph of the spiral coupling slit used in the experiment, with the measurement area marked by a dashed square. Inset scale bar is 10 microns. (b) Measured normalized probability distribution of post-interaction electrons as a function of the rotation angle of a quarter waveplate placed outside the UTEM. As the plate rotates (rotation angle is written above every measurement), the electron gradually transforms from a 2nd-order Bessel mode to a 0th-order Bessel mode, existing in a superposition of both modes at any intermediate step. Our results also suggest that such a scheme can be used to actively control not only the shape, but also the angular momentum quantity of the electron wavepacket. Three representative distributions are also presented in a larger magnification (with the measurement area marked by a dashed red line), clearly showcasing the difference in shape. The short and long white scale bars correspond to 2.5 and 0.5 microns, respectively. Other experimental parameters are the same as in fig. 1.

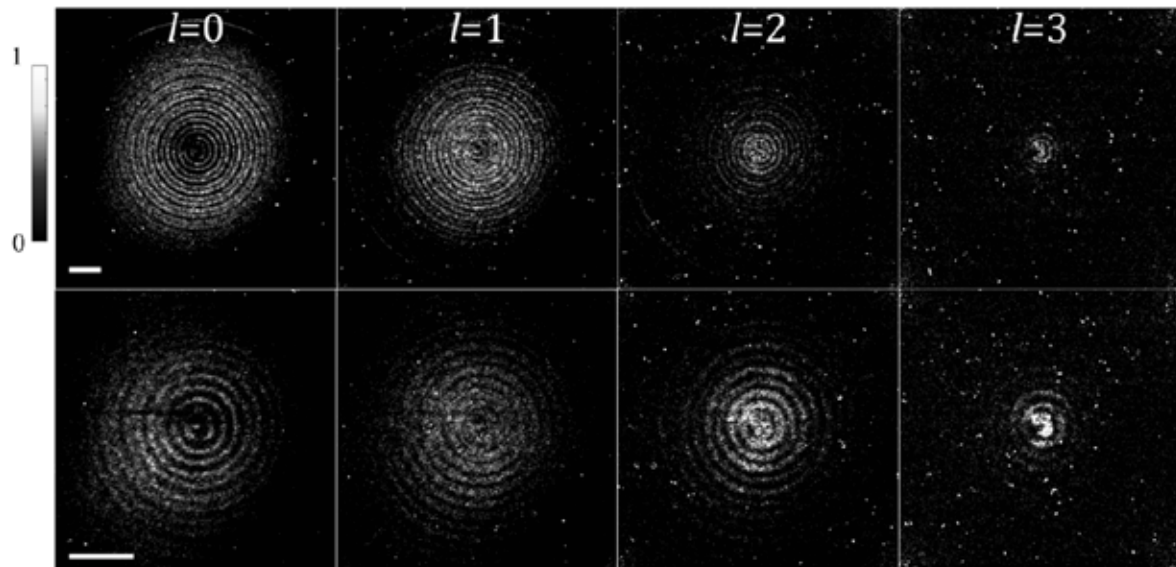


Fig. 3. Intensity-tunable photo-induced spatial modulation of electrons in the nonlinear interaction regime. Measured electron probability distribution for different interaction orders l , using a sharp electron energy filter (1 eV wide) around the interaction energy ($l \times \hbar\omega$, $\hbar\omega=1.7$ eV). Laser pulse intensity and temporal width were changed to 50 mW and ~ 660 fs, respectively. The distributions are presented both in a larger field of view (upper row) and at a larger magnification, exposing more delicate details (lower row). The short and long white scale bars both correspond to 2 microns. It is clear that the functional dependence of the interaction orders is different, as the level occupation of the electron is periodically modulated in the manner of Rabi oscillations. It is noteworthy that in the nonlinear interaction regime, the 0th order interaction contains features well below the plasmonic wavelength ($\lambda/7$ in our case, as measured at the central lobe).

References

- [1] J. Verbeeck et al., *Nature* **467**, 301 (2010).
- [2] Grillo, V. et al., *Phys. Rev. X* **4**, 011013 (2014).
- [3] R. Shiloh et al., *Ultramicroscopy* **144**, 26 (2014).
- [4] I. Madan et al., *Sci. Adv.* **5**, 8358 (2019).
- [5] G. M. Vanacore et al., *Nat. Mater.* **18**, 573 (2019).
- [6] A. Konečná and F. J. G. de Abajo, *Phys. Rev. Lett.* **125**, 30801 (2020).
- [7] Feist, A. et al., *Phys. Rev. Res.* **2**, 043227 (2020).
- [8] J. Verbeeck et al., *Ultramicroscopy* **190**, 58 (2018).
- [9] W. Cai et al., *Phys. Rev. B* **98**, 45424 (2018).
- [10] Feist, A. et al., *Nature* **521**, 200–203 (2015).
- [11] Wang, K. et al., *Nature* **582**, 50–54 (2020)

Smart Ghost Imaging

F. Grenapin¹, D. Paneru¹, T. Guner¹, A. D'Errico¹ and E. Karimi¹

¹*Department of Physics, University of Ottawa, Ottawa, ON, K1N 5N6, Canada*

Introduction

The performance of any imaging system is constrained by factors such as the level of illumination required, presence of background noise, and the optical resolution limits. For instance, in microscopy, the imaging of light-sensitive materials has been a persistent problem due to the risk of damaging the sample by the probe illumination. One can reduce the intensity of the light probing the sample: however, it comes with a trade-off in the Signal to Noise Ratio (SNR), which reduces the image quality and makes the noise significant. Another important metric of any imaging system is its resolution limit. Direct imaging schemes employing intensity measurements are severely limited in their resolution by the size of the optical apertures used. Recent advances in the field of “quantum imaging”, in particular, quantum illumination and ghost imaging (GI) protocols, have shown exciting promise in addressing these issues inherent in classical imaging.

Methods

“Quantum ghost-imaging” exploits the spatial correlations between photon pairs generated through the spontaneous parametric down-conversion (SPDC) process, significantly reducing the background noise, and producing images with reduced level of required illumination [1]. The term “ghost” refers to the fact that the image is formed with photons that have not themselves interacted with the object. In a variation of this technique using nondegenerate photon pairs, the image detection and sample interaction can happen at different wavelengths, which can be useful when imaging sensitive tissues when limited in detection technologies [2]. Furthermore, combining quantum detection techniques such as interaction-free measurement with GI, the illumination level required for the same levels of SNR in images [3] is significantly reduced.

Results

Along the direction of enhancing the image resolution, quantum metrological schemes have been shown to address the resolution limits inherent in intensity measurements, promising enhancement beyond the Rayleigh limit [4-6]. In this direction, one of our current works on super-resolution aims to enhance the resolution of GI protocols employing a high degree of spatial correlation between photon pairs and using phase sensitive projective measurements to analyze the modal content of the down converted light. Additionally, augmenting these novel techniques with machine learning, in particular, deep learning architectures such as Convolutional Neural Networks (CNNs), significant improvements can be observed in the image reconstruction, and object identification [7]. One of our work focuses on reconstructing images of biological samples from their edge enhanced ghost images employing

autoencoder deep learning architecture. Introducing an Orbital Angular Momentum (OAM) filter, one can obtain edge enhancement in the images. Edge enhanced GI has been shown to reduce the number of photons required to image any given sample as compared to conventional GI.

Discussion

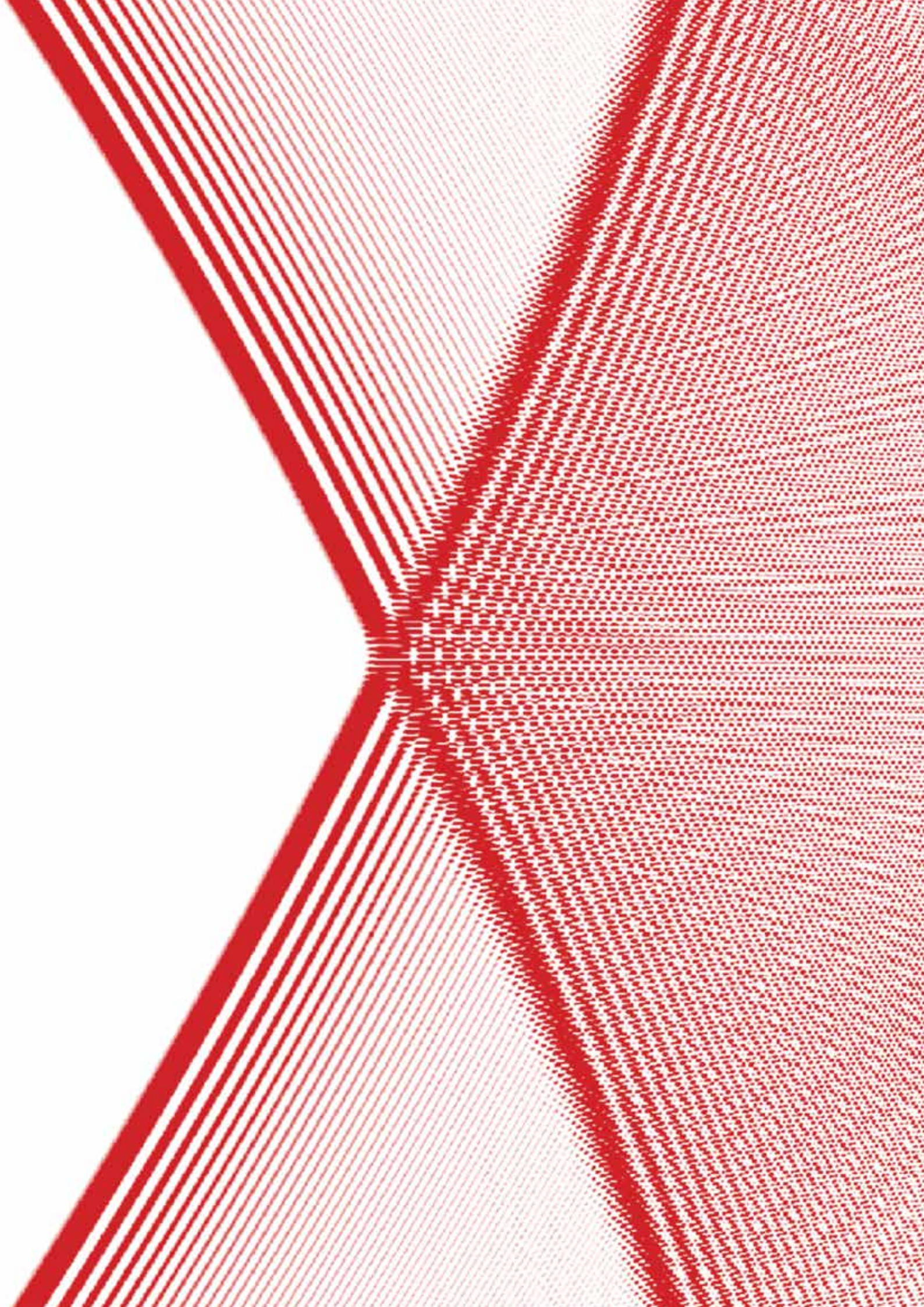
Here, we aim to provide an overview of different experiments currently carried out in our laboratory in the direction of enhancing resolution and efficiency of ghost imaging protocols.



Fig. 1 Examples of ghost images taken with entangled photon pairs.

References

- [1] Shapiro, J. H. & Boyd, R. W. (2012). The physics of ghost imaging. *Quantum Information Processing*, **11**, 949-993
- [2] Chan, K. W. C., O'Sullivan, M. N., & Boyd, R. W. (2009). Two-color ghost imaging. *Physical Review A* **79**, 033808.
- [3] Zhang, Y., Sit, A., Bouchard, F., Larocque, H., Grenapin, F., Cohen, E., Elitzur, A., Harden, J. Boyd, R., Karimi, E (2019). Interaction-free-ghost-imaging of structured objects. *Optics Express* **27**, 2212-2224.
- [4] Unternährer, M., Bessire, B., Gasparini, L., Perenzoni, M. and Stefanov, A., (2018). Super-resolution quantum imaging at the Heisenberg limit. *Optica* **5**, pp.1150-1154.
- [5] Tsang, M., Nair, R., Lu X., (2016). Quantum Theory of Superresolution for two Incoherent Optical Point Sources, *Physical Review X* **6**, 031033.
- [6] Zhou, S., & Jiang, L. (2019). Modern description of Rayleigh's criterion. *Physical Review A* **99**, 013808.
- [7] Lyu, M., Wang, W., Wang, H., Wang, H., Li, G., Chen, N., & Situ, G. (2017). Deep-learning-based ghost imaging. *Scientific Reports* **7**, 1-6.



Session H:

Ideas
and projects

Towards quantum electron wavepacket spectroscopy in the SEM

Albert Polman

NWO-Institute AMOLF

Science Park 104, 1098 XG Amsterdam, the Netherlands

Introduction

Free electrons in the scanning electron microscope (SEM) can undergo strong coupling to optical near fields at the nanoscale. Their relatively low velocity (10-30% of the speed of light) enables effective phase matching with the 10-50 nm spatial features of resonant optical modes in metasurfaces and nanoparticles at optical frequencies – a prerequisite for efficient energy exchange between electrons and light. Here, we present a new time-resolved SEM instrument designed to probe a wide range of electron-light-matter interactions by cathodoluminescence (CL) spectroscopy and photon-induced near-field electron microscopy (PINEM) using 1-30 keV electron energies.

New SEM-CL-PINEM microscope

Our microscope is equipped with a Schottky field-emission electron source and an electrostatic beam blanker to generate electron pulses with a controlled 30 ps - 10 ns duration. Spectral and angle-resolved CL measurements are acquired on a CCD array detector, and photon statistics are collected using a Hanbury-Brown and Twiss interferometer with 70 ps temporal resolution. For PINEM experiments, we use a near-infrared Nd:YVO laser emitting 1 ns optical pump pulses ($\lambda=1064$ nm, 1-25 kHz) that can be focused down to a 15- μm -diameter spot on the sample by a high-NA parabolic mirror. An electrostatic retarding-field analyser (RFA) is integrated into the SEM, allowing us to resolve laser-induced electron energy-gain and loss events with 100 meV energy resolution. For our pulsed electron beam, we find an intrinsic energy width of less than 800 meV, as primarily governed by the thermal spread of the Schottky field emitter gun. The spatial and temporal synchronization of electron and laser pulses is achieved by an ultra-fast InGaAs sensor that is directly integrated into the RFA detection unit.

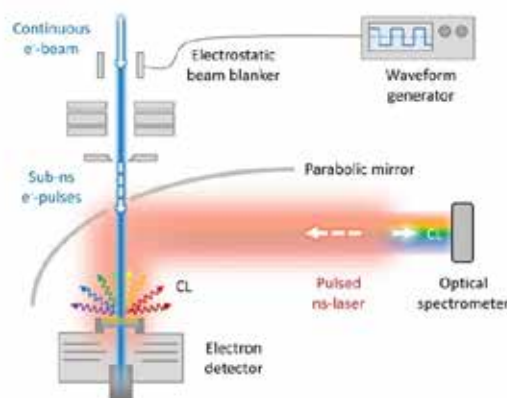


Fig. 1 SEM-CL-PINEM microscope design. A pulsed laser excites the metasurface that is irradiated with 1-30 keV electron pulses generated using an electrostatic beam blanker.

Electrons performing Fourier transforms

We first present a comparison of spectrally-resolved CL experiments at 2, 10 and 30 keV incident energy on 70-nm single-crystalline Ag nanocubes. We find distinct differences in the plasmonic dipole and quadrupole excitation rates depending on electron energy. At low energy, the electrons primarily interact with high spatial frequency Fourier components in the modal near-fields ($k=11k_0$), favoring the excitation of the tightly-confined quadrupolar cube modes. Vice versa, at 30 keV ($k=3k_0$) we mostly excite the dipolar modes, that show slower spatial variations that give smaller effective momentum components. By systematically studying the plasmonic mode intensities in the 1-30 keV range and performing a Fourier analysis, we derive for the first time a CL reconstruction of the optical mode field profile $E(z)$ along the electron trajectory.

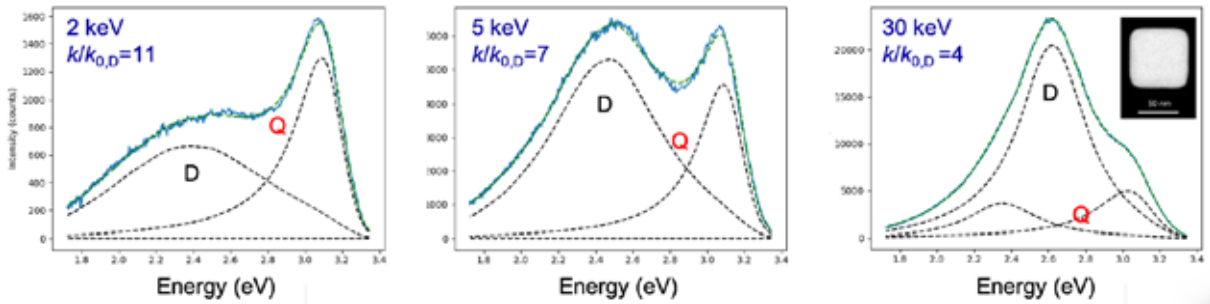


Fig. 2 CL spectra of Ag nanocubes at 2, 5, and 30 keV. Dipole and quadrupole resonance excitation efficiencies depend strongly on electron energy, reflecting the different matching of the modal spatial frequencies with the electron speed.

Optimizing the electron-plasmon interaction strength

To further study low-energy CL and PINEM interactions we design a holey metallo-dielectric metasurface with a tailored spatial near-field profile, optimized to enhance the interaction with 5 keV incident electrons. Figure 2a shows a simulated optical field distribution through a cross cut of the proposed layer geometry. The spectrum of spatial frequencies that describes the near field within the hole is shown in Fig. 2b. The data are expressed in terms of the electron-light interaction strength for varying electron energy (color scale). A pronounced interaction maximum is observed at the design energy of 5 keV.

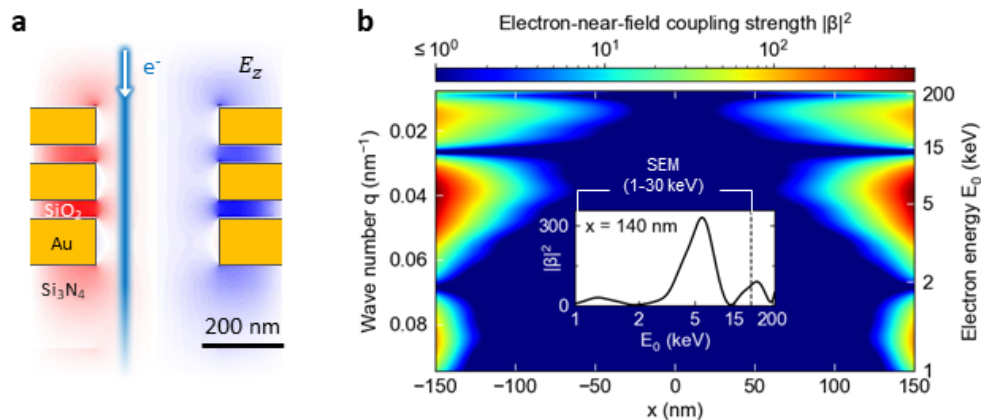


Fig. 3 Tailored optical near fields. **a** Simulated distribution of the parallel component of the optical field along the electron trajectory induced in a layered metallo-dielectric holey metasurface upon excitation by 1064-nm laser pulses. **b** Spatial frequency spectrum of the

optical field distribution within the hole versus hole radius with the corresponding electron energy on the right vertical axis. The color scale represents the electron-near-field coupling strength for an incident laser power density of 600 MW/cm².

Optical metasurface electron waveplate

We then introduce a novel optical phase plate concept to tailor the electron wavepacket in space and time. We exploit our insights in optical metasurfaces, that we typically use to control optical field distributions in the spatial domain. We design a square array of nanoscale holes with strong resonant near fields in the holes. The coherent superposition of PINEM interactions on a single electron across the hole array metasurface can then create an optical phase plate to achieve wide control over the electron wavepacket in space and time. We show calculations of this effect and aim to present to first experimental results towards this goal. The PINEM metasurface phase plate will enable entirely new ultrafast pump-probe detection schemes of optical excitations and relaxations. Moreover, it may create an alternative way to perform aberration corrections (in SEM and TEM) using spatial light modulation.

The new low-energy SEM-CL-PINEM-SEM technique opens up many applications of electron microscopy in integrated optics, nanophotonics, and opto-electronics and may provide detailed insights into the fundamental quantum nature of electron-light-matter interactions that have been experimentally inaccessible thus far.

SMART-electron: Dynamically modulating electrons' wave properties opening new frontiers in electron microscopy

G. M. Vanacore

Department of Materials Science, University of Milano-Bicocca, Milano, Italy

Addressing the grand-challenges that the world is facing nowadays in connection with 'energy', 'information' and 'health' requires the development of unconventional methods for unprecedented visualization of matter. SMART-electron aims at developing an innovative technological platform for designing, realizing and operating all-optical rapidly-programmable phase masks for electrons. By introducing a new paradigm where properly synthesized ultrafast electromagnetic fields will be used for engineering the phase space of a free-electron wave function, we will be able to achieve unprecedented space/time/energy/momentum shaping of electron matter waves, surpassing conventional passive monolithic schemes and revolutionizing the way materials are investigated in electron microscopy. Such unique high-speed, flexible and precise full-phase multidimensional control, will enable novel advanced imaging approaches in electron microscopy with enhanced features, such as higher image-resolution, lower electron dose, faster acquisition rate, higher signal-to-noise ratio, and three-dimensional image reconstruction, together with higher temporal resolution and high energy-momentum sensitivity. In SMART-electron, we will make such potential a reality by implementing for the first time three beyond-the-state-of-the-art imaging techniques enabled by our photonic-based electron modulators, namely: (1) Ramsey-type Holography, (2) Electron Single-Pixel Imaging, and (3) Quantum Cathodoluminescence. Such new approaches will lead to unprecedented visualization of many-body states in quantum materials, real-time electrochemical reactions, and spatio-temporal localization of biomimetic nanoparticles in cells for drug delivery. By surpassing the current paradigms in terms of electron manipulation, the project has the potential to drive electron microscopy into a new and exciting age where scientists will benefit from new tools with unprecedented performances that were unimaginable until now.

A FEW NEW IDEAS FOR FUTURE DIRECTIONS OF MICROSCOPY

V.Grillo

S3, Istituto di nanoscienze-CNR, Modena, Italy

Introduction

This work is aimed to wrap up about the QSORT project and propose a route of future developments.

With QSORT a few important results have been achieved and others are at close reach. We have been able to demonstrate a new complex electro-optics element namely the electrostatic Orbital Angular Momentum (OAM) Sorter [1], to produce the first EELS-OAM 2D spectra and to apply that to the orbital mapping of 2D material like h-BN, we are getting close to atomic scale EMCD and we have already studied it theoretically[2].

In the development of these ideas we learned new things like how to use machine learning for the first time to auto align a custom optics in an electron Microscope [3], how to use MEMS to create custom electron optics for many forms of beam shaping, how to describe theoretically a scattering in the OAM basis and how to generalize the concept of conformal transformations in microscopy [4].

At the same time we are getting close to reach experimentally atomic scale EMCD and reaching new results about plasmon scattering of structured electrons.

We have also deployed the OAM Sorter in the low dose analysis of proteins obtaining a compression of information and the potential to study details of sensible material without needing to fully image them.

The first part of this presentation will be dedicated to illustrate some of these recent results that are reported in fig. 1. However I would like to illustrate new ideas and possible directions.

MINEON

One direction I would like to push forward is the idea of custom optics based on MEMS can be carried on beyond the case of the OAM sorter. First of all we can create more elements like spiral phase plates as innovative phase plates, new phase plates for conformal mapping and, with some further developments, spherical aberration correction and other classical complex elements could be designed. For this the ability to align innovative electron optics elements at different planes must be conjugated with a detailed and reliable MEMS manufacturing and design..

For this reason, for example, we devised new experimental ways to create boundary conditions (see fig. 2 left) based on current dividers and a mathematical description of thin

electrodes phase plates producing a numerical recipe on how set the value of the voltages. All of this will be at the basis of the project MINEON that just started [5].

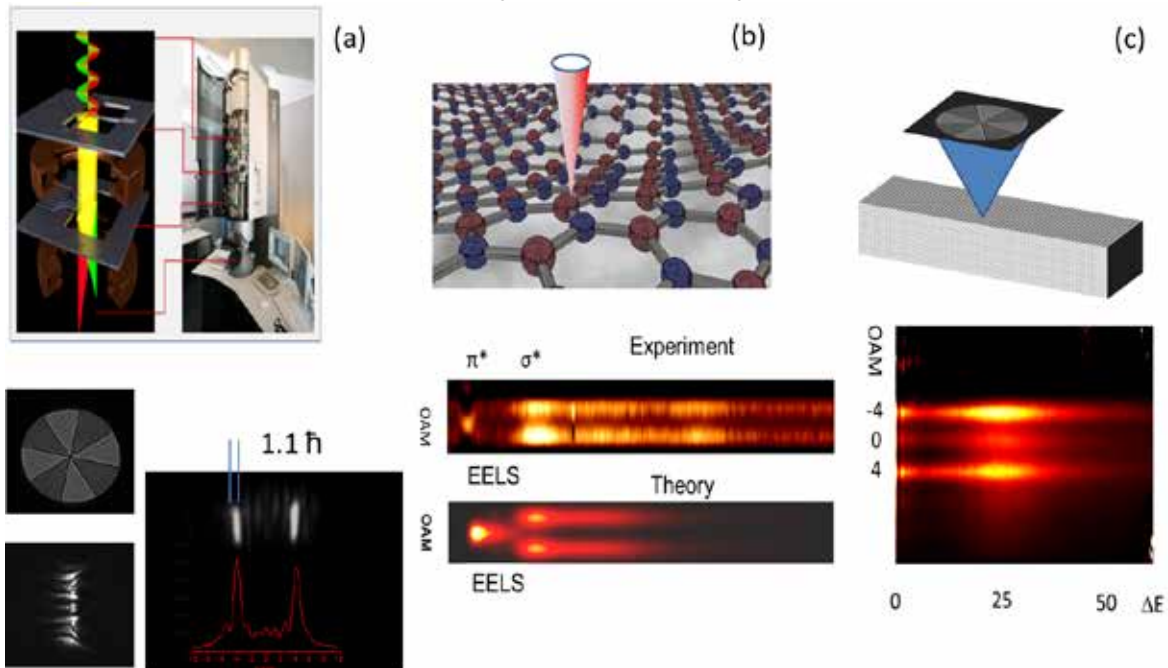


Figure 1. (a) OAM sorter configuration in an electron microscope, the near ideal resolution of 1.1 quanta of OAM can be reached. (b) Experimental data of OAM and energy loss measurement on h-BN revealing the symmetry of the σ and π transitions (c) Experimental data on volume plasmon energy loss and OAM with a structured illumination.

GHOST IMAGING

Another idea that I believe will be interesting to pursue is the idea of looking at the inelastic scattering with a new perspective.

In “low loss” inelastic scattering we are always looking at the electron disregarding the excited quasi particle. However a new scheme allows to gain more information using the auxiliary concept of Ghost imaging and a simple quasi particle detector.

The concept is inspired by light optics. In optical “ghost imaging” [6],[7], an entangled photon pair (or classically correlated photons) is sent along two different paths. One follows a path where both the object and a bucket detector are located consecutively, while the other is sent to a spatially-resolved detector such as CCD camera. The coincident measurement of the bucket detector and CCD camera results in the formation of an image of the sample on the CCD camera. The counter-intuitive result is the photons on the CCD camera never passed through the sample.

This same scheme can be used to describe the correlation between electron and collective excitations leading to an image in the electron detector post selected by the coincidence with a detection for example of a surface plasmon polariton [8]. The whole scheme is depicted in fig 2 (right).

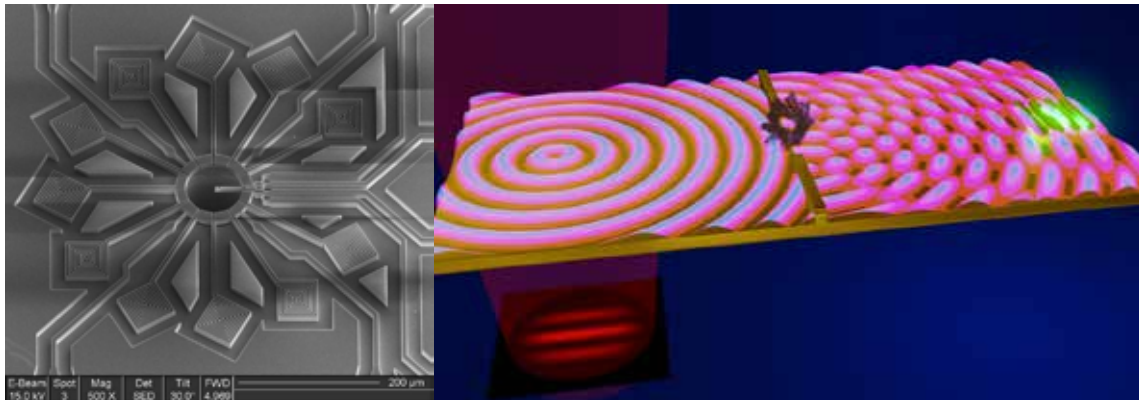


Figure 2 (left) MEMS phase plate with the new scheme for smooth boundary conditions based on current dividers (right) the idea of ghost imaging to look at molecules in “near field” interaction free condition.

Conclusion

In conclusion the work of these years has shown there is still a lot of work to be done and the most promising idea come from the full exploitation of the quantum nature of the electrons and at the same time of the creation of new “unconventional” optical elements controlled by advanced neural network.

References

- [1] A.H. Tavabi et al. Phys. Rev. Lett. **126**, 094802 (2021)
- [2] E. Rotunno et al. Physical Review B **100**, 224409 (2019)
- [3] E. Rotunno et al. Ultramicroscopy **213**, 113338 (2021)
- [4] G. Ruffato et al. Physical Review Applied **15** (5), 054028 (2021)
- [5] <http://www.mineon.eu>
- [6] Padgett M.J. and Boyd R.W. An introduction to ghost imaging: quantum and classical Phil. Trans. R. Soc. A. **375**, 20160233, (2017)
- [7] Gatti A., Brambilla E., Bache M., Lugiato L.A. Ghost imaging with thermal light: comparing entanglement and classical correlation. Phys. Rev. Lett. **93**, 93602, (2004).
- [8] E. Rotunno et al. arXiv:2106.08955 (2021)

